*Published in Progress in Aerospace Sciences* ***41*** *(2005) 471-453*

# SCRAMJETS AND SHOCK TUNNELS – THE QUEENSLAND EXPERIENCE

R.J. Stalker[1], A. Paull[2], D.J Mee[3], R.G. Morgan[4] and P.A. Jacobs[5]
Mechanical Engineering, University of Queensland, Brisbane, Qld 4072

## ABSTRACT

This article reports on the use of a shock tunnel to study the operation of scramjet powered configurations at sub-orbital velocities above 2 km/s. Thrust, as given by a net thrust equation, is used as a figure of merit throughout the study. After a short description of the shock tunnel used and its operating characteristics, experiments on the combustion release of heat in a constant area duct with hydrogen fuel are reviewed. The interaction between heat release in the combustion wake and the walls of the duct produced pressure distributions which followed a binary scaling law, and indicated that the theoretically expected heat release could be realized in practice, albeit with high pressure or long combustion ducts. This heat release, combined with attainable thrust nozzle characteristics and a modest level of configuration drag, indicated that positive thrust levels could be obtained well into the sub-orbital range of velocities. Development of a stress wave force balance for use in shock tunnels allowed the net thrust generated to be measured for integrated scramjet configurations and, although the combination of model size and shock tunnel operating pressure prevented complete combustion of hydrogen, the cruise condition of zero net thrust was achieved at 2.5 km/s with one configuration, while net thrust was produced with another configuration using an ignition promoter in hydrogen fuel. Nevertheless, the combination of boundary layer separation induced inlet choking and limited operating pressure levels prevented realization of the thrust potential of the fuel. This problem may be alleviated by recent increases in the shock tunnel operating pressures, and by promising research involving inlet injection of the fuel.

Research on the drag component of the net thrust equation resulted from the development of a fast response skin friction gauge. It was found that existing theories of turbulent boundary skin friction predicted the skin friction when combustion of hydrogen occurred outside the boundary layer, but combustion within the boundary layer dramatically reduced the skin friction. Finally, for the first time in the world, supersonic combustion was produced in a free flight experiment. This experiment validated shock tunnel results at stagnation enthalpies near 3 MJ/kg.

## KEYWORDS

Scramjets, Shock Tunnel, Free Flight Supersonic Combustion, Hypersonic Propulsion, Turbulent Boundary Layers, Shock Tunnel Instrumentation

[1] Corresponding author. Em. Professor
[2] Professorial Fellow
[3] Associate Professor
[4] Professor
[5] Senior Lecturer

## NOMENCLATURE

| | | |
|---|---|---|
| $A$ | = | flow cross-sectional area ($m^2$) |
| $A_\infty$ | = | frontal area ($m^2$) |
| $C_D$ | = | drag coefficient = $2D/\left(\rho_\infty U^2 A_\infty\right)$ |
| $C_{TN}$ | = | thrust coefficient = $2T_N/\left(\rho_\infty U^2 A_\infty\right)$ |
| $C_j$ | = | injected fuel thrust coefficient |
| $D$ | = | drag ($N$) |
| $e_n$ | = | nozzle efficiency = thrust/(one-dim. nozzle thrust) |
| $F$ | = | thrust function |
| $g$ | = | gravitational acceleration ($m/s^2$) |
| $I_{sp}$ | = | specific impulse (sec) |
| $M$ | = | Mach number |
| $M_c$ | = | Mach number after combustion heat release |
| $n$ | = | $\Delta T/T_{NN}$ = combustion duct + thrust nozzle efficiency |
| $p$ | = | pressure ($Pa$) |
| $P_c$ | = | pressure after combustion heat release ($Pa$) |
| $\Delta Q$ | = | heat released by fuel combustion in air (= 3.45 MJ/kg for stoichiometric hydrogen) |
| $T_N$ | = | net forward thrust ($N$) |
| $T_{NN}$ | = | net forward thrust when all of combustion heat release is converted to stream kinetic energy ($N$) |
| $\Delta T$ | = | thrust increment with one-dimensional nozzle ($N$) |
| $U$ | = | freestream velocity (m/s) |
| $\gamma$ | = | ratio of specific heats |
| $\theta$ | = | flow direction |
| $\theta_D$ | = | initial nozzle divergence angle |
| $\nu$ | = | Prandtl-Meyer function |
| $\rho$ | = | density ($kg/m^3$) |
| $\rho_\infty$ | = | freestream density ($kg/m^3$) |

## 1. INTRODUCTION

Half a century ago it seemed that airbreathing hypersonic flight was a prospect for the not-too-distant future. At that time supersonic missiles which used ramjet propulsion were in operation, and it seemed almost inevitable that they would be succeeded by missiles which, by employing supersonic combustion, would enter the hypersonic speed regime. By providing operational experience, these missiles would be the prelude to the emergence of piloted hypersonic vehicles, leading in turn to the emergence of an airbreathing orbital spaceplane.

Although this scenario did not appear unduly optimistic at the time, and may even reflect the sequence in which developments will ultimately occur, the time scales of a few years implicitly assumed for these developments have turned out to be hopelessly awry. For a number of reasons, some economic and some technical, progress towards airbreathing hypersonic flight has been slow.

Supersonic combustion was demonstrated in the laboratory and incorporated in missile designs during the 1960's[(1)]. Although these designs were tested in wind tunnels and associated combustion test facilities, they were never flown. During the 1970's and 1980's the NASA Langley Research Centre conducted an extended program of research related to airframe integrated scramjets for flight at Mach 7. This involved development of combustion hypersonic wind tunnels and design of vehicle components[(2)]. In the late 1980's and early 1990's, the NASP design study explored the feasibility of extending the knowledge base gained up to Mach 7 to near Earth-orbital

Mach numbers of 25. It was found that new knowledge was required to produce a successful design of vehicle which would operate up to these Mach numbers.

Thus, until recently, the exploitation of supersonic combustion to reach hypersonic Mach numbers had been confined to design studies and wind tunnel experimentation. Supersonic combustion had not occurred in flight until July, 2002, with the University of Queensland "HyShot" flight experiment, and it had not been used in an engine which propelled a flight vehicle until the NASA "Hyper-X" flight of March, 2004.

A significant aspect to the Hyper-X flight is that the knowledge which had been built up through a sustained program of wind tunnel experimentation and development led to an engine which operated successfully the first time it was tried in flight. This is encouraging, because a factor which had inhibited the development of airbreathing hypersonic flight was that extreme expense of flight testing, and the ability to ensure a high degree of success by wind tunnel testing makes the expense of a flight development program more manageable. The same would apply to flights with a more basic (and less expensive) objective, such as the HyShot flight, where the probability of a successful flight experiment was enhanced by shock tunnel experiments.

It is clear that the further development of airbreathing hypersonic flight will be bound up with the use of wind tunnel type facilities. For experiments involving supersonic combustion facilities which simultaneously produce flight values of temperature and velocity are required. Observing that Earth orbital velocity stands as a notional limit for scramjet operation, a useful figure of merit for a scramjet wind tunnel is the ratio of the airstream kinetic energy per unit mass to that of an airstream at orbital velocity. When this ratio exceeds 0.1, which occurs at an airstream velocity of approximately 2.5 km/sec, a wind tunnel may be regarded as "sub-orbital". The combustion wind tunnels which are being used to open up the Mach 7 to 8 flight regime are hypersonic but, by this definition, are not sub-orbital.

The airstream velocities that can be produced in these combustion hypersonic facilities are limited by the further requirement for supersonic combustion that the combustion chamber density must be high enough to ensure that combustion takes place within a reasonable length. Experience with combustion of hydrogen in air suggests that, typically, a density of the order of 0.05 $kg/m^3$ would be required for essentially complete mixing and combustion in a combustion chamber 0.5 m. long at a flow velocity of 2 km/sec and a precombustion temperature of 1000 K. If such a combustion chamber were part of a scramjet engine with an inlet area contraction of 5, the test section power level per unit area of a wind tunnel to test this engine would be of the order of 100 $MW/m^2$. Wind tunnel power levels of this order are usually obtained by operating in the "blow down" mode, where the energy is stored over a period of time in a combination of high pressure receivers and storage heat exchangers, and released in a much shorter time period, usually of the order of seconds, often with extra energy added by combustion[(3)]. This form of intermittent operation has been favoured for scramjet wind tunnels for the Mach 7 to 8 regime, but is unsuitable for the sub-orbital regime.

Scramjet wind tunnels for the sub-orbital regime are required to operate with airstream velocities exceeding 2.5 km/sec and, since test section power levels per unit area increase as the cube of the airstream velocity, it is clear that, even with intermittent operation, the power levels required for operation in the sub-orbital regime are very large. Added to that, the temperatures involved in supplying air at those velocities exceed 3000 K, which makes operation in the blowdown mode very difficult. Therefore it is unlikely that blowdown, intermittent, technology can be applied to sub-orbital scramjet wind tunnels except, perhaps, with the most generous access to resources.
An alternative means of achieving high wind tunnel power levels, which be seen as an extreme extension of the blowdown technique, is to very rapidly add energy to the test gas immediately before it is allowed to expand to produce the test section flow. With these "impulse" techniques

steady test section flow conditions persist for only a few milliseconds, but higher test section power levels and supply temperatures can be sustained during that time, than with intermittent wind tunnels. Therefore it is possible to use these techniques in penetrating the sub-orbital regime. The impulse technique which has gained widest acceptance is the shock tunnel, and the use of a shock tunnel for scramjet research is the subject of this article.

It should be mentioned at the outset that the level of penetration into the sub-orbital regime that is achieved with a shock tunnel is limited by the pressures at which the test gas can be contained prior to expansion, and will depend on whether the shock tunnel is used for component research or for experiments with integrated configurations. The expansion tube is an impulse technique which offers a means of overcoming this limitation, but is still in the very early stages of development. Not withstanding the pressure limitation, the shock tunnel offers a particular opportunity of exploring the effects of increasing velocity on airbreathing propulsion related phenomena, and this has been exploited for the research at the University of Queensland. In doing this, it has been recognized that shock tunnel instrumentation is not as developed as for intermittent tunnels, and therefore a substantial effort has been directed towards the development of novel instrumentation, suited to millisecond test times, which is required for this research.

Australian scramjet research was reviewed some years ago[4], and the reader may wish to refer to that review for a more detailed account of scramjet experiments at the University of Queensland. The present article provides an update on the Queensland research and its interpretation, as well as indicating how it influenced the development of shock tunnel instrumentation.

The article begins with a brief discussion on the reduced effectiveness of combustion heat release which increased penetration into the sub-orbital regime implies, and the way this has influenced the direction of research. After a description of the operation of the free piston shock tunnel at the University of Queensland, and of the scramjet shock tunnel work which preceded it, the article goes on to consider scramjet component research, which initiated work at the University of Queensland. A study of simple integrated configurations followed, which led on to further component research and a flight experiment.

## 2. PERFORMANCE AT SUB-ORBITAL VELOCITIES

The difficulty of operating in the sub-orbital regime increases with velocity, because a characteristic of airbreathing engine operation is that the energy added by combustion yields a progressively smaller propulsive effect as the airstream velocity becomes larger. This is illustrated by a simplified one-dimensional flow analysis based on the diagrammatic vehicle configuration shown in Fig. 1. Here the flow streamtube is the same area at capture and exit and, in passing through the engine, the combustion energy release $\Delta Q$, is added to the flow. The vehicle experiences a drag $D$, and a net forward thrust $T_N$, which is the difference between the thrust developed and the drag. The net thrust coefficient is obtained by neglecting the pressure difference between capture and exit, equating $\Delta Q$ to the kinetic energy gain of the flow through the engine, and using the momentum balance to yield the relation

$$C_{TN} = 2\left\{\sqrt{1+2\Delta Q/U^2}-1\right\}-C_D .$$

For hydrogen and for hydrocarbon fuels in stoichiometric proportions, $\Delta Q \leq$ 3.45 MJ/kg, indicating that it is a sufficient approximation in the sub-orbital regime to take $\Delta Q/U^2 << 1$, and, taking the first two terms in $\Delta Q/U^2$ in a Taylor series expansion of $\sqrt{1+2\Delta Q/U^2}$, to write

$$C_{TN} = \left(2\Delta Q/U^2\right)\left(1-0.5\Delta Q/U^2\right) - C_D, \qquad (1)$$

as the first version of the net thrust equation for a scramjet.

**(Figure 1 here)**

$C_{TN} = 0$ for a vehicle in the cruise phase, while for a vehicle in the boost phase, $C_{TN}$ forms a product with the flight velocity which is proportional to the net fuel specific impulse, and therefore is a measure of the efficiency with which fuel is used in acquiring vehicle velocity. In both cases, the reduction in the first term on the right hand side of eqn (1) as the velocity increases implies that a corresponding reduction in the second term must take place to maintain performance. This becomes more difficult as the velocity increases. Therefore research at sub-orbital velocities must not only seek efficient combustion and expansion of the combustion products in the thrust nozzle, in order to realise an effective value of $\Delta Q$ which is as close to the theoretical value as can be achieved, but must also consider the minimization of $C_D$. The manner in which the experiments developed to reflect this philosophy will be apparent below.

## 3. PRIOR SHOCK TUNNEL SCRAMJET TESTS

To the authors' knowledge, the first shock tunnel experiments on supersonic combustion occurred in 1962[5], and demonstrated both mixing controlled combustion and reaction controlled combustion. The first published account of scramjet experiments in a shock tunnel is due to Osgerby et al, in 1970[6]. They used a two-dimensional model consisting of a single ramp intake followed by a constant area combustion chamber and, using hydrogen fuel, they were able to observe supersonic combustion at low equivalence ratios. Unfortunately, their experiments were done in a conventional shock tunnel operating in the tailored interface mode with helium driver gas, and therefore they were limited to test section velocities of 2.1 km/sec. This implied that when the test gas precombustion temperature was raised to 1160 K, in order to obtain combustion within the length of their combustion chamber, the precombustion Mach number was only 2.1, and thermal choking of the combustion chamber occurred as the equivalence ratio exceeded 0.2. In spite of this choking limit their experiments were a valuable pioneering work, as they demonstrated that the short test times available with a shock tunnel did not preclude scramjet experiments.

## 4. THE FREE PISTON SHOCK TUNNEL T4

By using a free piston shock tunnel, it was possible to produce higher sub-orbital velocities than could be achieved by a conventional shock tunnel with helium driver gas, and thus to operate at higher equivalence ratios without thermal choking. Free piston shock tunnels were first introduced at the Australian National University, in Canberra, and early research by the Queensland group was conducted by visits to Canberra to use the ANU shock tunnel. However, the construction of the free piston shock tunnel T4 at the University of Queensland enabled the group to continue their work there. Only T4 will be described here, as it embodies the same principles of operation as all free piston shock tunnels, and is the one most relevant to the University of Queensland research.

**(Figure 2 here)**

T4 is shown in general arrangement in Fig. 2(a). A free piston is used to compress and heat the shock tube driver gas. A piston with a mass of 92 kg is normally used and, referring to the figure, is launched from the right hand end of the compression tube, which is 26 m. long and 228 mm. in diameter, and initially contains the shock tube driver gas. The piston is driven along the compression tube by the expansion of air initially contained in the piston driver reservoir, which has a volume of 1.2 $m^3$ and a maximum working pressure of 14 MPa. The piston acquires kinetic energy as it is driven along the compression tube, and this energy is then passed to the shock tube driver gas as the piston slows down on approaching the left hand end of the compression tube. The

driver gas is adiabatically compressed to pressures which are a multiple of the initial pressure in the piston driver reservoir. A high pressure diaphragm, located at the left hand end of the compression tube, spontaneously ruptures when the shock tube driver gas reaches a predetermined pressure. This initiates conventional operation of the shock tube, which is 10 m. long and 75 mm. in diameter. The resulting shock wave in the test gas traverses the length of the shock tube and reflects from its left hand end, where it ruptures a thin Mylar diaphragm to initiate the flow of test gas through the nozzle and test section. The shock heated test gas thus becomes the supply gas for the nozzle and test section flow, with a nozzle supply pressure which could somewhat exceed 50 MPa on a routine basis, for the experiments discussed here. This limit has lately been raised to 90 MPa.

### 4.1 Test Times – Driver Gas Contamination of the Test Flow

Typical records of test section pitot pressure and nozzle supply pressure are shown in Fig. 2(b). A rule of thumb used in shock tunnel research is that the test flow must traverse three model lengths in order for the mainstream and boundary layer flows to effectively reach a steady state. The stagnation enthalpy of the figure yields a flow velocity of about 3.5 km/sec, indicating that the flow would reach a steady state on a model one metre long in 0.9 milliseconds. Thus the pitot pressure record indicates that a steady state flow persists for about 1.3 milliseconds or 4.5 model lengths. However, the figure also shows the arrival of driver gas contamination of the test flow and, if the experiment in the shock tunnel demands uncontaminated test flow, then steady flow persist for only 0.5 milliseconds, or 1.8 model lengths, and only test results obtained in this time can be accorded unqualified acceptance. Thus the useful test time in a shock tunnel may be determined by driver gas contamination, rather than by the time for which the nozzle supply pressure remains unchanged.

Measurements of the time to contamination in T4 are presented in Fig. 2c. The measurements were first made using a time of flight mass spectrometer[7], and later with a shock detachment probe[8]. The latter was developed as a simple instrument for routine monitoring of the test flow, and works by choking a duct when the specific heat of the flow gas increases beyond a critical value. It will be noted that the 10% contamination test time is reduced to zero for stagnation enthalpies in excess of 15 MJ/kg. It is thought that this may be due to turbulent mixing at the interface between the test gas and the driver gas in the shock tube. The peculiarities of the shock tunnel site demanded a length to internal diameter ratio of the shock tube of 133, instead of the value of 80 to 100 used in normal shock tunnel practice, and the extra length may have allowed extra mixing to take place. Notwithstanding this effect, it will be seen below that the test times available at stagnation enthalpies somewhat less than 15 MJ/kg have proven adequate for scramjet research so far.

### 4.2 Fuel Supply

Hydrogen fuel was used for almost all the tests referred to here, and was supplied to a model in the test section from a room temperature reservoir. For safety reasons, the capacity of the reservoir was limited so that it contained less than 35 litres of free hydrogen at its maximum working pressure of 10 MPa. The supply of hydrogen to the test section was controlled by a quick acting solenoid valve, which was slaved to the recoil of the compression tube to open and start fuel injection on the model approximately 10 milliseconds before flow was initiated in the test section. Thus a constant rate fuel flow was established on the model before the test flow arrived. Fuel was injected through pre-calibrated orifices at the model, and the fuel flow was monitored by pressure transducers located as near the injection orifices as was conveniently possible.

### 4.3 Early Experiments

It was clear that, as scramjet research developed, it would involve interaction of mainstream pressure fields with the boundary layer. Two early series of experiments provided reassurance that a steady flow involving such effects could be produced in the short test times available in the shock tunnel.

The first of these series of experiments involved the glancing interaction of a weak shock with a boundary layer. This interaction was expected to be a common feature of scramjet duct flows, and was represented by glancing interaction of a weak shock with a laminar boundary layer at a Mach number of 5.6[9]. Pressure distributions were used to demonstrate that a steady interaction could be produced within 0.5 milliseconds with a characteristic model dimension of 0.3 m. The second series of experiments involved pressure and heat transfer measurements on the upper, leeward, surface of an 0.2 m long model of the Space Shuttle Orbiter[10], and comparison with flight measurements on the vehicle itself, to provide data on the three-dimensional separated flows which prevailed in that region. These data indicated that steady flow was produced in that region and, when Reynolds number effects were taken into account, the pressure and heat transfer distributions matched those obtained in flight.

It was recognised that these experiments did not cover all the possible boundary layer related flows which could occur in a duct, particularly those involving relatively large two-dimensional separated regions. However, they provided preliminary assurance that, provided such extreme flow situations could be avoided, duct flows with pressure gradients could be expected to reach a steady state in the short test times of a shock tunnel.

### 4.4 Steady flow for Scramjet Experiments

Further assurance that steady state scramjet flows could be produced in shock tunnel test times was provided as more results became available. Figure 3 shows two examples of these results. The first, shown in Fig. 3(a), involved combustion in a constant area combustion duct which, with a length of 1.2 m. and 48 x 100 mm. cross-section, was relatively large in comparison with the 250 mm. nominal test flow diameter. An hydrogen injection strut was located at the mid-plane of the duct spanning the 100 mm. dimension. The pressure distributions indicate a steady flow over the duct length, with the exception of the first of the fuel-on pressure distributions, taken 0.9 milliseconds after shock reflection, which reaches the steady state at all but the two downstream stations. The fuel-on pressure distributions reach a complete steady state 0.3 milliseconds later. The flow velocity was 3.3 km/s, and the steady state persisted for at least 0.6 milliseconds, which was therefore sufficient for an element of the mainstream flow to pass at least two model lengths.

**(Figure 3 here)**

The second example, shown in Fig. 3(b), relates to the thrust produced by a simple nozzle downstream of a rectangular constant area duct. The overall length of the model was one metre and the nozzle was made by deflecting one wall of the downstream 0.475 m. of the duct at a divergence angle of 11 degrees, to become the thrust surface of the nozzle. This surface was instrumented with 24 pressure transducers and, by integration of the measured pressures over the surface while allowing for the surface angle, the thrust at any instant could be obtained. The variation of the thrust with time is displayed in Fig. 3(b). The time scale is referenced to the same origin as Fig. 2(b), and therefore the test period begins at approximately one millisecond. To a close approximation, the thrust is seen to remain steady for the subsequent one millisecond interval.

## 5. SUPERSONIC COMBUSTION IN A DUCT

Combustion in a supersonic duct flow is at the heart of scramjet operation, and a considerable effort was devoted by the University of Queensland group to investigation of this phenomenon at sub-orbital speeds. It was appreciated that the length of the duct should be as short as possible, whilst allowing for mixing and combustion of the hydrogen fuel with air. Duct divergence would tend to produce falling temperatures in the flow direction along the duct and, because of the exponential dependence of temperature of the reaction rates, would tend to require elongation of the combustion chamber for combustion to be reasonably complete. On the other hand, convergence of the duct

would tend to produce additional drag, due to the combustion pressure rise acting on the duct surface, and also would tend to encourage choking of the duct. Thus the investigation of supersonic combustion was centred on constant area ducts. These also offered the advantage of some simplicity in interpreting results of the experiments.

The chemical release of energy may cause choking of the duct in two ways, and a simplified discussion, based on the Rayleigh flow model for heat addition in a constant area duct, serves to illustrate the manner in which the combustion chamber flow may be affected.

The first way in which choking can occur is thermal choking. This occurs when sufficient thermal energy is added to a supersonic flow in a duct to reduce the flow Mach number to one. The flow is then unable to accept additional thermal energy, and any attempt to further add energy results in a reduction of the mass flow through the duct, and a consequential spilling of surplus mass flow from the duct entrance. The flow is then said to be choked. A flow which has just reached the choking condition, in a constant area duct, can be described by the equation for a Rayleigh flow (e.g. Ref. 11) and, provided that the precombustion Mach number in the duct is at least at high supersonic levels, the precombustion velocity is approximately related to the heat release by

$$U^2 = 2\left(\gamma^2 - 1\right)\Delta Q, \qquad (2)$$

where $\gamma$ is an average value of the ratio of specific heats during the heat release process. The maximum value of $\Delta Q$ is 3.5 MJ/kg for hydrogen fuel in air, and therefore, with $\gamma$ = 1.3, the maximum value of $U$ for which thermal choking will occur is 2.2 km/sec. Making some notional allowance for the approximate nature of the analysis, it may be concluded that thermal choking will only occur at the lower bound of the sub-orbital regime, if at all in that regime.

The second way in which heat release causes choking is through the boundary layer interacting with the mainstream. A sufficient increase in pressure in the direction of mainstream flow will cause the boundary layer to separate, thereby reducing the effective duct cross-sectional area for the mainstream flow. If the area reduction is large enough to reduce the local Mach number to one, the flow becomes choked and, similar to the case of thermal choking, any attempt to increase the pressure rise along the duct results in spilling of surplus mass flow from the duct entrance. A criterion for this to occur can be formulated by noting that the density levels required for combustion imply that duct boundary layers are turbulent, and the pressure at which a two-dimensional turbulent boundary layer will separate is given by the approximate relations of Korkegi[12] as

$$P_i/p = 1 + 0.3\left(U/a\right)^2 \text{ for } U/a < 4.5 \qquad \text{(a)} \qquad (3)$$

and

$$P_i/p = 0.17\left(U/a\right)^{2.5} \text{ for } U/a > 4.5 \qquad \text{(b)}$$

where $P_i$ is the incipient separation pressure and $p$ and $a$ are the pressure and speed of sound at which the boundary layer originates. As will be seen below, the latter is an important point in relation to scramjets, since parts of the boundary layer in the combustion chamber may originate at the intake leading edge. However, for the present purpose, the boundary layer origin is taken to be at the duct entrance. Though eqns (3) are intended to apply to two-dimensional flow, the tentative conclusion reached in tests reported below is that it may also apply to the three-dimensional flow which is typical of a scramjet duct, and this will be assumed to hold for the present discussion.

Thus by comparing the pressure rise given by eqns (3) with that which accompanies combustion energy release, it is possible to determine whether boundary layer separation, and possible resultant

choking, may occur. An approximate combustion pressure rise may be obtained by again using a Rayleigh analysis[11], with the square of the Mach number much greater than one both before and after the heat addition zone, to yield

$$p_c/p \approx 1 + (\gamma - 1)\Delta Q/a^2 \qquad (4)$$

where $p_c$ is the downstream pressure. For upstream temperatures of 880 K to 1200 K, representing a possible range of ignition temperatures of hydrogen in air, the speed of sound in air ranges from 550 m/sec to 670 m/sec, and with $\Delta Q$ = 3.5 MJ/kg and $\gamma$ = 1.3, $p_c/p$ ranges from 4.5 to 3.3. Equations (3) then indicate that the combustion induced pressure rise will not separate the boundary layer at upstream velocities above approximately 2.0 km/sec. Thus, this type of choking in a constant area duct is only expected to occur at the lowest velocities of the sub-orbital regime. However it is worthwhile reiterating that this will not apply when the combustion chamber is preceded by an intake which subjects the boundary layer to a preliminary pressure rise.

## 6.0 THE TWO-DIMENSIONAL COMBUSTION WAKE

Equation (4) indicates that the addition of fuel to a supersonic airstream in a duct, and the mixing and combustion which follows, will generate an increase in pressure along the duct. This pressure increase leads to thrust generation in an expansion nozzle which follows the duct, and therefore it was important to develop some understanding of the means of generating this pressure increase. This was done by studying combustion wake phenomena in relation to the pressure rise in a duct of rectangular cross section with a central injector spanning the duct, as shown in Fig. 4(a), to produce a flow which was essentially two dimensional. The two dimensional configuration was chosen because it offered relative simplicity for interpretation of experimental results. It was recognised that this configuration may not be the most efficient one, in terms of providing maximum combustion in minimum combustion chamber length.

**(Figure 4 here)**

### 6.1 Wake Independent of Duct Height

The mechanism by which the duct pressure rise was produced was investigated experimentally using the configuration of Fig. 4(b)[13]. The precombustion pressure in the duct was 61 ± 5 kPa, the Mach number was 4.4 ± 0.2, the stagnation enthalpy was varied from 5.6 MJ/kg to 8.9 MJ/kg, and the associated air velocity varied from 2.9 km/s to 3.5 km/s, while hydrogen fuel was supplied from a room temperature reservoir at a velocity of 2.3 ± 0.1 km/s. Duct heights of 30, 50 and 70 mm. were used, and the fuel flow rate was maintained at a value corresponding to an equivalence ratio of one with a 30 mm. duct height.

The inset on the top right of Fig. 5 shows typical pressure distributions obtained when hydrogen fuel was injected into air and nitrogen. These were obtained under conditions corresponding to a precombustion temperature of 1480 K. The difference in the pressure distributions is ascribed to combustion, which clearly causes the fuel-air wake to produce a much greater pressure rise than the fuel-nitrogen wake. As indicated by the straight lines on the figure, the pressure increases linearly with distance downstream. Estimates of the ignition length for a hydrogen-air mixture[14] indicate that this length is less than an order of magnitude less than the length of the duct, indicating that the growth of the wake is governed by the process of mixing between hydrogen and air, rather than the reaction process.

**(Figure 5 here)**

A numerical analysis of this flow[13], based on the two dimensional model of Fig. 4(a), found that the growth of the wake displacement thickness was responsible for the combustion induced increase in pressure along the duct and, as illustrated in Fig. 5, the growth in displacement thickness was independent of the height of the duct. The figure shows that, using the same combustion wake, a reasonable prediction can be made of the pressure rise along the duct by subtracting the sum of the displacement thicknesses of the wake and the boundary layers on the walls of the duct from the duct cross sectional area, implying that as the duct height reduces, the mainstream experiences greater contraction and the pressure rise is increased. This model breaks down for the 30 mm. duct at a temperature of 1230 K, where it overpredicts the pressure rise but, for the less extreme conditions, it is possible to regard the development of the wake as decoupled from the associated pressure rise.

### 6.2 Mass Spectrometer Wake Traverses

Decoupling of the formation of the wake and the pressure distributions implied that experiments on a wake which was free of wall constraints would yield information applicable to the ducted wakes of interest. Traverses of such a free wake were made at a downstream distance of 500 mm. from hydrogen injection, with a pitot rake and with a time of flight mass spectrometer[15]. By sampling the flow through a 2 mm. orifice and a conical skimmer system, the mass spectrometer was able to provide a traverse of species concentrations in the wake. The wake was formed at a mainstream Mach number of 5.5 ± 0.3, and the measured wake thickness remained approximately constant at 40 mm. as the mainstream temperature was varied from 760 K to 1,750 K. Hydrogen was injected at equivalence ratios exceeding one, based on an imaginary duct height of 50 mm.

It was found that the amount of hydrogen mixed with air in stoichiometric proportions was 75% ± 20% of the hydrogen which would be injected at an equivalence ratio of one, despite the fact that the relative amounts of injected hydrogen increased with temperature, the equivalence ratio reaching 2.2 at the highest temperature. Thus, to the first order, the proportion of mixed hydrogen and air in the wake was unaffected by a surplus of hydrogen. The proportion of mixed hydrogen which reacted to form water increased with mainstream temperature, reaching 50% at the highest temperature. This was in accord with reaction rates based on the mainstream temperature and pressure[14]. In order to avoid unwanted electrical discharges in the mass spectrometer it was necessary to limit the static pressure to values of 20 kPa or less in these experiments. Raising the pressure to two or three times those levels, as in the duct experiments above, can be expected to lead to nearly complete combustion of the mixed hydrogen.

As may be expected, hydrogen concentrations were highest at the centre of the wake, where they caused the average molecular weight to fall to values of 9.8 ± 0.5, compared with mainstream values of 27 to 29[16]. Pitot pressure profiles were in approximate accord with the profiles of average molecular weight, indicating that the distribution of the hydrogen concentration was the major factor influencing the wake pitot pressure profile.

### 6.3 Scaling of Supersonic Combustion

Scaling studies are not only important for extrapolating from laboratory experiments to flight, but they can be helpful in revealing the dominant phenomena in a flow system. Experiments were done to compare the pressure distributions in the two ducts shown schematically in Fig. 6(a)[17]. To ensure the same composition of test gas entering the two ducts, the large duct was supplied with oblique shock recompressed flow from a Mach 8 shock tunnel nozzle, and the small duct was supplied directly from a Mach 4 nozzle. The ducts were geometrically similar, but different in size by a factor of 5, the large duct height being 47 mm., and the small duct, 9.4 mm. Precombustion pressures in the large duct varied from 25 kPa to 10 kPa, and from 101 kPa to 32 kPa in the small duct, while the precombustion Mach number was 4.4 ± 0.2, and the hydrogen fuel equivalence ratio was 1.3 ± 0.2.

**(Figure 6 here)**

At each flow condition, the values of the product of the duct precombustion pressure and the duct height was the same for the two ducts. The results presented in Fig. 6(b) show that, by setting this product to be the same, identical normalized pressure distributions in the large duct and the small duct are obtained when the distance downstream of injection is scaled by the duct height. Thus, binary scaling applies to these flows, implying that small scale experiments can be used as models of larger scale flows.
The pressure distributions on the right hand side of the figure indicate the effect of varying the precombustion temperature while the precombustion pressure remains approximately constant, as indicated by the nozzle reservoir pressure on the figure. The linear pressure distributions, with the pressure gradient reducing as the precombustion temperature increases, indicate mixing controlled growth of the combustion wake, as in Fig. 5. It might be noted that Figure 5 is also associated with linear pressure distributions at precombustion temperatures as low as 1230 K.

The left hand side of Fig. 6(b) indicates the effect of varying the precombustion pressure, as indicated by the values of nozzle reservoir pressure on the figure, while maintaining the precombustion temperature at 1100 ± 50 K. The gradient of the pressure rise along the duct is somewhat reduced as the precombustion pressure falls, but the most notable feature of these pressure distributions is that they do not exhibit the linear characteristic of those at higher temperatures. This non linearity is consistent with the expected rapid increase in the flow length for reaction, which occurs as the mainstream temperature falls at about the temperature of these pressure distributions. At these temperatures the reaction length is sufficiently large that, in comparison with the mixing controlled flows on the right hand side of Fig. 6(b), the combustion release of energy is delayed, allowing more mixing and creation of radicals to take place, before a delayed but rapid energy release and relatively steep pressure rise. Thus, the pressure distributions on the left hand side of Fig. 6(b) represent examples of reaction controlled combustion.

Reaction controlled combustion wakes were observed in other experiments. It was found[18] that raising the precombustion pressure at a precombustion temperature of 1200 K in the large duct would lead to the expected reduction in the combustion energy release delay but, as less mixing had then occurred, the combustion pressure rise was reduced. With a 25 mm. duct height, and precombustion pressures exceeding 150 kPa, the combustion energy release delay was further reduced[19], but the pressure rise was such as to suggest substantial combustion energy release, and hence enhanced mixing. This may have been associated with the occurrence of a normal shock which was observed in the fuel rich part of the wake[20]. Other experiments[21] have shown that the interaction between a shock wave and a wake can lead to enhanced mixing.

Equation (4) with $\Delta Q$ = 3.45 MJ/kg provides an estimate of the resultant pressure levels if all the oxygen in the air entering the duct is burnt, and this level is shown on Fig. 6(b) for each pair of pressure distributions. The duct lengths are just sufficient for complete combustion, except at the highest precombustion temperature, where it is expected that the combustion energy release, $\Delta Q$, will be limited by partial dissociation of the combustion products.

6.4 Thrust and Specific Impulse Potential

The thrust which arises from heat release in the combustion chamber may be determined by using the thrust function, which is the sum, at any station, of the stream flux of momentum and the impulse of the pressure force. For a one dimensional flow the thrust function may be written (Ref. 11, p. 113)

$$F = pA\left(1+\gamma M^2\right) \qquad (5)$$

For inviscid flow in a duct of varying area, the thrust on the walls of the duct between two stations, 1 and c (see Fig. 7(b)), is equal to the difference between the thrust functions at the two stations. For the constant area combustion duct considered here, where no thrust is generated at the walls of the duct, the thrust function must remain constant along the duct, and therefore the Mach number is reduced as the pressure is raised by combustion, according to the relation

$$M_c^2 = \left\{\left(1+\gamma M_1^2\right) P_1/P_c - 1\right\}\Big/\gamma \qquad (6)$$

A comparison between the Mach number obtained from eqn (6) and experimental Mach number distributions in a 50 mm. high duct is shown in Fig. 7(a). The experiments were done at an equivalence ratio of 0.75 and a precombustion temperature, Mach number, pressure and velocity of 1200 K, 5.1, 41 kPa and 3.54 km/sec respectively[22]. The Mach number distribution was obtained from cross stream pitot surveys, coupled with the assumption of constant static pressure across the duct. For this figure, the pressure $P_c$ is regarded as the pressure at any station in the duct and varies linearly along the duct as the combustion energy release increases. The corresponding Mach number, $Mc$, is calculated from eqn (6) and $\gamma = 1.3$. As shown in Fig. 7(b), the station 1 corresponds to precombustion conditions.

**(Figure 7 here)**

Although the peak values of Mach number are close to the precombustion value near the walls of the duct, the Mach number at the centre of the duct approaches $M_c$, and the width of the central region where this applies grows, as the distance from injection increases. The mass spectrometer wake traverses, which have already been discussed, show relatively high hydrogen concentration at the centre of the duct, indicating the approach to the Mach number $M_c$ in that region is taking place more rapidly than the hydrogen is mixing with air. Thus, as the duct becomes longer, the flow at the downstream end of the duct can be expected to exhibit a growing central region where the Mach number $M_c$ applies, with shrinking regions close to the wall, where higher Mach numbers occur, before the Mach number falls again in passing through the wall boundary layer. For a fully mixed flow, in the absence of boundary layers, the central region extends across the duct cross section. Such a flow is assumed for input to the expansion/thrust nozzle in Fig. 7(b).

Using eqn (4) for $P_c/P_1$, with eqn (6) for $M_c$, and assuming one-dimensional flow in the thrust nozzle with $\gamma = 1.3$, the change in the thrust function corresponding to the nozzle area ratio $A_3/A_2$ can be used to calculate the thrust delivered by the nozzle for both the precombustion Mach number $M_1$ (i.e. the thrust delivered in the absence of heat release), and the combustion Mach number $M_c$. The difference between these can be used to yield the normalized thrust increment due to combustion, $\Delta T/p_1A_1$. This thrust increment can be compared with that obtained when all of the combustion energy release is converted into stream kinetic energy through use of the exact form of eqn (1), with omission of the drag term, $C_D$. Neglecting the small change in the stream velocity in passing through the intake in Fig. 7(b), this yields

$$T_{NN}/p_1 A = \left(\gamma/a_1^2\right)\left\{\sqrt{1+2\Delta Q\Big/\left(a_1^2 M_1^2\right)} - 1\right\} \qquad (7)$$

which can be expressed in terms of $p_c/p_1$, the ratio of the combustion pressure at the end of the combustion duct to the precombustion pressure, by using eqn (4). Then, making the comparison between $\Delta T$ and $T_{NN}$, with $\gamma = 1.3$, yields the results shown in Fig. 7(c) for $\Delta T/T_{NN}$, the ratio of

the incremental thrust obtained with the idealised configuration of Fig. 7(b) to that obtained if perfect conversion of combustion energy release into stream kinetic energy takes place. Thus, denoting this ratio as *n*,

$$n = \Delta T / T_{NN} \ . \qquad (8)$$

This is plotted in Fig. 7(c) for a range of precombustion Mach numbers and selected values of the nozzle area ratio, $A_3/A_2$. The ratio *n* varied only slightly as $P_c/P_1$ changed from 5 to 2 for each nozzle area ratio, a variation which is accommodated by the cross hatched bands shown in the figure.

Figure 7(c) shows that, even with an infinite thrust nozzle area ratio, when no thermodynamic energy is retained in the exhaust gases, only approximately 60% of the combustion energy release is available to produce thrust. Noting that the nozzle exit area cannot be substantially bigger than the capture area without producing excessive drag, and that choking of the inlet due to boundary layer separation, as indicated by eqns (3), will limit the inlet contraction ratio, a thrust nozzle area ratio of 10 could be taken as a reasonable working value, and this implies that approximately 40% of the combustion energy release is available to produce thrust. Thus it is appropriate to rewrite eqn (1) as

$$C_{TN} = \left(2n\,\Delta Q/U^2\right)\left(1 - 0.5\,\Delta Q/U^2\right) - C_D \, . \qquad (9)$$

This is the second version of the net thrust equation for a scramjet. The difficulty of achieving high velocities in the sub-orbital regime was remarked on in relation to eqn (1). Since values of *n* are substantially less than one, eqn (9) indicates further exacerbation of that difficulty.

Equation (9), with $C_D$ omitted, can be used to estimate a stoichiometric hydrogen fuel specific impulse by again assuming that the stream velocity is constant in the inlet and the frontal area, $A_\infty$, is equal to the capture area. This gives the specific impulse, $I_{sp}$, as

$$I_{sp} = 34.4\,n\,\Delta Q/(gU)\left\{1 - 0.5\,\Delta Q/U^2\right\} \qquad (10)$$

which, with $\Delta Q$ = 3.45 MJ/kg, and *n* = 0.4, yields a specific impulse varying from 1300 sec at a velocity of 3.0 km/sec to 800 sec at 6.0 km/sec. Net specific impulses of the order of 1000 sec are desirable in the sub-orbital regime, and it is clear that attention must be paid to the drag if this is to be achieved.

The specific impulse of eqn (10) can be seen as an incremental specific impulse, or the specific impulse corresponding to the incremental thrust due to combustion. With *n* = 0.32, corresponding to a thrust nozzle area ration of 5, eqn (10) is compared with experimental measurements in Fig. 8. Two sets of measurements are shown, both sets involving a 50 mm. wide two dimensional combustion duct and thrust nozzle combination. One set involved a relatively long combustion duct as shown schematically at the top of the figure [23]. The model illustrated may be seen as an experimental embodiment of Fig. 7(b), without the inlet. It had a thrust nozzle area ratio of 4.3, which is close enough to 5 for the present purpose. Hydrogen was injected through a central strut. The precombustion pressure, Mach number, and fuel equivalence ratio were 100 kPa, 4.4 and 1.0 respectively, and the velocity was adjusted by varying the test flow stagnation enthalpy. Thrust was measured by integrating the pressures measured by 25 transducers over the thrust surface, and was converted into a specific impulse using the measured mass flow of injected hydrogen.

**(Figure 8 here)**

The other set of measurements was taken in the free piston shock tunnel at the Australian National University, in Canberra[24], with a similar configuration, but with a combustion duct length of only 175 mm., which is approximately one third of that shown in Fig. 8. The height of the combustion duct was 25 mm., the thrust surface angle relative to the combustion duct axis was 15°, and the thrust nozzle area ratio was 4. The precombustion pressure, Mach number and fuel equivalence ratio were 110 ± 20 kPa, 3.6 ± 0.15 and 1.0 respectively. Both sets of results are plotted against freestream velocity, which is calculated as the square root of twice the stagnation enthalpy. Although the results for the shorter combustion duct tend to be slightly less than those for the longer one, implying that somewhat less mixing and combustion may have taken place in that case, there is reasonable overall consistency between experiment and theory, indicating that eqn (10) provides a first order estimate of the potential incremental specific impulse of hydrogen fuel in the sub-orbital regime.
It is worthwhile drawing attention to the effect of thrust nozzle area ratio in these experiments. For example, if, instead of a thrust nozzle area ratio of 5, an area ratio of 20 were used, yielding a value of $n = 0.45$ in eqn (10), the theoretical specific impulse in Fig. 8 would be increased by 40%, and would only fall below 1000 sec. as the velocity exceeded 5 km/sec.

6.5 Fuel Injection

The experiments discussed so far have all involved a central injector in the combustion duct, generating a duct flow that was essentially two dimensional. Whilst this has simplified interpretation of those experiments, it was appreciated that heat transfer considerations may preclude the use of an injector situated in the mainstream of the combustion duct flow, and therefore that other modes of injection should be considered.

First, injection through a slot at the wall was investigated[25], measuring pressure and heat transfer distributions with a combustion duct height of 25 mm., width of 50 mm. and length from injection of 400 mm. It was found that the combustion induced pressure rise along the duct was only 30% to 60% of the precombustion pressure. Although this pressure rise was much less than with the central injector, the injection of hydrogen along the wall nevertheless had the anticipated effect of substantially reducing the heat transfer. A numerical model was developed which yielded results consistent with the observed pressure rise and heat transfer. This numerical model indicated that the main factor limiting the combustion pressure rise was weak mixing of the hydrogen and air, with only approximately 20% of the hydrogen being mixed at the downstream end of the duct. This may be compared with the mass spectrometer measurements of section 6.2, which indicated that about 75% of the hydrogen was mixed at 500 mm. downstream of a central injector.

Thus wall injection through a single slot would require a much longer combustion duct to achieve the same levels of mixing and combustion as a central injector. It may be argued that the central injector involves two mixing layers, on either side of the two dimensional combustion wake, whereas the surface slot involves only one, and a proper comparison would involve two slots, one each on opposing walls of the duct. Assuming that the amount of hydrogen mixed is independent of the equivalence ratio for each slot, as suggested by the mass spectrometer results, it would be expected that 40% of the hydrogen would be mixed at 400 mm. with the two slot configuration. Taking this a step further, to consider four slots on the walls of a duct with a 50 mm. square cross section would lead to approximately 80% of the hydrogen mixed at 400 mm. This is comparable with the amount of hydrogen mixed at 500 mm. with the central injector. Thus a suitable arrangement of surface slot injectors is likely to produce a combustion pressure rise which is similar to that for central injection in about the same length of combustion duct. The surface slot injectors

also have the advantage that they reduce heat transfer and skin friction, a phenomenon which will be discussed further below.

Next, injection from a wall orifice was investigated[26] and results were compared with those obtained for central strut injection. The experiments with central injection were done in the duct of Fig. 4(b), with a duct height of 30 mm, while those with a wall orifice were done with a duct of similar dimension, but with a duct height of 25mm. This ensured that both ducts were able to capture the same freestream flow area. Noting that the streamwise component of injection velocity adds significantly to overall thrust, a hydrogen injection angle of 30° with respect to the freestream direction was chosen, thereby retaining 87% of the possible injection thrust. Hydrogen was injected through a 7 mm diameter sonic orifice located in the centre of the wider wall of the duct. Figure 9(a) shows results obtained at a precombustion pressure, velocity and temperature of 66 kPa, 3.1 km/s and 1480 K respectively, with hydrogen injected from a room temperature reservoir at an equivalence ratio of one for both types of injection. The results of numerical calculations for the central injector are also presented, in order to illustrate the scatter in the pressure measurements caused by the presence of the injection strut. The pressure measurements for wall injection were taken on the centreline of the wider wall of the duct, and would be subject to three dimensional flow effects which would be expected to decay with downstream distance. These sources of uncertainty make it possible to discriminate between the pressure increases due to the two types of injection with an accuracy of only roughly ± 20% but, to within that accuracy, it is clear that both types of injection produce the same combustion induced pressure increase.

**(Figure 9 here)**

A limited investigation of mixing and combustion using multiple wall orifices was also undertaken[27] and indicated that, while multiple orifices offer an increase of the order of 30% in the streamwise rate of pressure rise alone, this was not a sufficient improvement to encourage further experiments.

Finally, the effect of the stagnation temperature of the injected hydrogen was investigated. This is of interest because it is anticipated that a hydrogen fuelled scramjet vehicle would use the hydrogen as a coolant before it was injected into the combustion duct, and this would raise the hydrogen stagnation temperature before injection. Experiments were conducted in which the hydrogen was heated by adiabatic compression immediately prior to injection[28]. Heating was accomplished by a "gun tunnel" type of apparatus, wherein a light piston rapidly compressed the hydrogen in a long tube, to produce a period, lasting a few milliseconds, during which the hydrogen was retained at constant pressure and temperature at the end of the tube. The gun tunnel was slaved to the shock tunnel so that, during this constant temperature period, injection of hydrogen into the test flow through the model in the shock tunnel took place. The model in the shock tunnel was again that shown in Fig. 4(b), with a duct height of 30 mm and a central injector. The injection Mach number was fixed by the internal injector contour, and therefore increasing the fuel stagnation enthalpy increased the fuel injection velocity, with effects as shown by the example in Fig. 9(b). Here hydrogen injection at stagnation temperatures of 300 K, 450 K and 700 K into a duct flow with a precombustion pressure, temperature and velocity of 65 kPa, 1230 K and 2.9 km/s, respectively, produces a streamwise rate of combustion induced pressure increase which is reduced as the difference between fuel velocity and the precombustion air velocity is reduced. This implies that a longer combustion duct will be required to achieve a given degree of mixing and combustion. At the highest fuel stagnation temperature, when the fuel and air velocities are essentially the same, the required combustion duct length is almost double that required when the fuel is supplied from a room temperature reservoir.

The comparison between injection from a single wall orifice and central strut injection was repeated with heated hydrogen fuel[26], with the same result as that obtained when the fuel was injected from a room temperature reservoir. The reduction of the streamwise rate of pressure rise as the fuel stagnation enthalpy increased was the same with the wall orifice as with the central injector, implying that the wall orifice will also require approximately double the combustion duct length for mixing and combustion as the fuel stagnation temperature increases from 300 K to 700 K.

### 6.6 Length of Combustion Duct

At this point it is worthwhile making some comment on the length of combustion duct required for complete combustion with a central injector. When the flow was mixing controlled a linear pressure distribution along the duct was obtained. Figure 6 indicates that a duct length exceeding 20 duct heights was then required to approach the theoretical levels of pressure increase, as given by eqn (4).

As explained in sub-section 6.1, the linear pressure distribution was due to the combustion induced displacement thickness of the wake reducing the flow cross-section available to the mainstream, causing the pressure to increase. It follows that the distribution of wake displacement thickness, and associated combustion heat release, was non-linear along the duct, the streamwise rate of combustion heat release reducing with increasing distance downstream. Thus small proportional reductions of the duct height may be expected to yield larger proportional reductions in duct length, or as shown in Fig. 5 for duct heights near 30 mm, proportionately larger increases in predicted pressure at a fixed station in the duct.

This non-linear growth in wake displacement thickness may partly explain why the experimental results of Fig. 8 indicate that duct lengths of 7 duct heights and 18 duct heights produce approximately the same propulsive effects, and why experiments with precombustion pressures in excess of 190 kPa and a combustion duct 25 mm high yielded nozzle pressure distributions indicating complete combustion in the duct with a duct length of 7 times the duct height[29]. Another possible explanation for the relatively short duct lengths for complete combustion is associated with the relatively low precombustion Mach numbers, of 3.4 ± 0.5, which prevailed in these experiments. It can be shown that this will lead to low post injection Mach numbers in the hydrogen core of the wake, thus encouraging the formation of normal shock waves which enhance mixing. This raises the possibility that further research may reveal advantages to using low post injection Mach numbers of hydrogen.

While the mechanism which yielded the shorter combustion duct lengths was not clear, it was not unreasonable to suppose that the interaction between the combustion processes and the fluid dynamics of the duct flow would follow the same scaling law as the longer duct lengths. Therefore, this scaling law was invoked in choosing the shorter combustion duct lengths for the experiments on integrated scramjet models which are described in further sections of this article.

Although much more work could be done to further improve our understanding of confined combustion wakes, the knowledge gained thus far is sufficient for designing simple scramjet combustion ducts, and allows attention to be shifted to other aspects of sub-orbital scramjet operation.

## 7. THE TWO DIMENSIONAL THRUST NOZZLE

The experiments of the previous section on the confined combustion wake indicated that the nominally two dimensional flow associated with the central injector configuration was, for practical purposes, as effective as the other injection modes tried in ensuring mixing and combustion of hydrogen in a minimum duct length. Thus, in considering a thrust nozzle to follow the combustion

duct, it was appropriate to retain the relative simplicity of two dimensional flow, and regard thrust nozzle performance in that context.

7.1 The Supersonic Thrust Nozzle

A two dimensional thrust nozzle flow is shown in Fig. 10(a). The nozzle expansion is formed by a corner and, after reflection of the resultant wave from the upper surface of the nozzle, the wave is cancelled at the thrust surface by the nozzle contour, to produce a flow which is parallel to the flow at nozzle entry. Supersonic nozzle design theory indicates that this is the shortest nozzle which will effect a given increase in area while producing a parallel exit flow. If the nozzle entry flow is not uniform, then the thrust function at the entry and the exit can be obtained by integrating the streamtube thrust function over the nozzle cross-section at the entry and exit respectively. However, if inviscid flow is assumed, and a completely mixed and burnt flow is supplied by the combustion duct, then the entry flow is uniform and parallel, and if the combustion products behave as a perfect gas during the nozzle expansion, so is the exit flow. The nozzle thrust for the combustion Mach number, $M_c$, can then be obtained by subtracting the entry thrust function from the exit thrust function, as for the one-dimensional nozzle of Fig. 7(b).

**(Figure 10 here)**

However, a difficulty then arises in obtaining the thrust increment due to combustion. As well as increasing the pressure at the nozzle entry, the combustion heat release also reduces the entry Mach number. But a contoured nozzle of given area ratio and initial divergence angle can only be designed to produce a uniform and parallel exit flow at one entry Mach number, so if the nozzle is designed to match the combustion Mach number, it will not match the pre-combustion Mach number. Thus the nozzle flow without combustion will generate expansion or compression waves passing out of the nozzle exit, manifested in an internal drag to partially offset the nozzle thrust. The nozzle thrust without combustion is therefore reduced and, when subtracted from the thrust with combustion, will yield a resultant thrust value in excess of the thrust increment due to combustion. The true value of the thrust increment due to combustion would be obtained by subtracting the thrust generated by a nozzle designed to produce uniform and parallel flow for the pre-combustion Mach number.

7.2 Nozzle Adjustment for Matching

As discussed in Ref. 24, the difficulty of matching a nozzle to two different Mach numbers can be avoided when the difference between the combustion and no-combustion entry Mach numbers is such that the difference between the initial divergence angles of matched nozzles is small. The entry flow may also be incompletely mixed and burnt. Beginning with a nozzle flow which is matched for the no-combustion flow, as shown in Fig. 10(b) (i), and using measured pressure distributions on the thrust surface, the difference between the combustion and no combustion pressures are converted into an increment in the Prandtl-Meyer function, $\Delta\nu$, according to the relation

$$\Delta\nu = \int \frac{\sqrt{M^2 - 1}}{\gamma M^2} \frac{dp}{p}. \qquad (11)$$

Then, using the relation $\nu + \theta$ = constant along (+) characteristics, and $\nu - \theta$ = constant along (-) characteristics, where $\theta$ is the flow angle, taken as positive in the clockwise direction, the distribution of $\Delta\theta$ necessary to eliminate wave reflection from the thrust surface is obtained and is used to adjust the nozzle contour. The matched nozzle for no combustion is thereby converted to a matched nozzle for combustion. By virtue of the adjustment in surface angle, the area ratio of the matched combustion nozzle is somewhat greater than the matched no combustion nozzle but,

provided that the required adjustment in surface angle is small, only a relatively small increase in the nozzle area will take place and, as shown in Fig. 7(c), the thrust is relatively insensitive to variation of area ratio in the range of interest here.

As illustrated in Fig. 10(b) (ii), the same method of suppression of the reflection of the combustion induced compression waves from the thrust surface may be applied to a nozzle with a straight thrust surface. Therefore a good approximation to the thrust increment due to combustion may be obtained with a straight nozzle by subtracting the no combustion thrust from the combustion thrust.

Estimates with $\gamma$ = 1.3 indicated that, for values of the combustion pressure ratio, $P_c/P_1$, approaching two, the difference between the initial divergence angles of matched nozzles was less than one third of the mean divergence angle, signifying that a difference of the order of one third in the nozzle area ratios will occur. Fig. 7(c) shows that such nozzle area variations lead to only a small variation in thrust.

7.3 Straight (ie Constant Divergence) Nozzles

When the value of the combustion pressure ratio exceeds two, the difference between the combustion and the no combustion Mach numbers becomes larger, and therefore the difference between the initial divergence angles of the matched nozzles reaches value that suggest significant variation in thrust. It then becomes necessary to consider nozzles with only small initial divergence angles. If the nozzle has a straight thrust surface, the centred Prandtl-Meyer expansion from the corner at the nozzle entry will be reflected from the upper nozzle surface, as shown in Fig. 10(a), and will be reflected again from the thrust surface. This process of reflection and re-reflection of the expansion wave from the corner will continue downstream as the nozzle expands. The magnitude of the change in flow angle across the wave remains equal to the small nozzle divergence angle, and thus there is a small increase of the thrust function across the wave each time the wave reflects and traverses the nozzle. At any of these reflections, the nozzle expansion can be terminated by suitable contouring, as shown in Fig. 10(a), to eliminate further reflections and generate a uniform and parallel flow. Contouring of the nozzle can be seen as adding a wave which cancels the reflected wave and, as the added wave will involve small changes in flow angle, it will also involve small changes in the thrust function. The thrust function of the contoured nozzle flow will be identical to a one dimensional nozzle flow at the same area ratio. Because the change in flow angle across the wave is small, the cross sectional area of the contoured nozzle will be approximately equal to the cross sectional area of the straight nozzle at a given station. Thus, since the thrust function and area ratio of the straight nozzle are closely approximated by the thrust function and area ratio of the contoured nozzle, the straight nozzle will also yield approximately the same thrust as a one-dimensional nozzle at the same area ratio. Now, contouring of the straight nozzle can be applied at any of the wave reflections that occur in the nozzle, and at each wave reflection the straight nozzle exhibits the same relation between thrust and area ratio as the one-dimensional nozzle. Therefore, by interpolating between wave reflections, the one-dimensional relations can be applied, in approximate form, to all of the straight nozzle.

An example of the error made in assuming one-dimensional relations between thrust and area ratio for a straight nozzle is given in Ref. 30. The example takes a relatively large nozzle divergence angle of 20°, with an entrance Mach number of 2.72 and an area ratio of 12. The nozzle thrust was calculated by a numerical procedure, and yielded a thrust which was 85% of that obtained with a one-dimensional calculation. For smaller nozzle divergence angles, one-dimensional calculations may be expected to result in even closer approximations to true values of thrust, provided that the entry Mach number is not too much greater than 2.72. Noting that the thrust increment due to combustion is obtained as the difference between combustion and no combustion thrust, and that this involves some cancellation of the errors made in employing the one-dimensional

approximation, the final value of the thrust increment due to combustion may be expected to be within a few percent of the value calculated with the one-dimensional approximation.

The experimental difficulty in matching nozzles to obtain the combustion thrust increment is thus avoided by accepting approximate values for the thrust increment. The experimental specific impulse values of Fig. 8 are derived from thrust levels which are measured by employing this approach. However, at the higher precombustion Mach numbers associated with flight at high sub-orbital speeds, this approximate approach to obtaining the combustion thrust increment is likely to require unacceptably small values of the nozzle divergence angle, and the problem of realizing the full combustion thrust increment in the thrust nozzle will remain. For a vehicle of fixed geometry in the boost phase, when Mach numbers in the engine vary continuously, the problem will become even more acute.

7.4 Non-uniform Mach Number Profile at Nozzle Entry

It has already been pointed out, in sub-section 7.2, that the entry flow may be incompletely mixed and burnt. In fact, this may be expected to be the more usual case, as an excessive duct length would be expected if mixing and combustion were to be completed before nozzle entry. An example of the type of entry flow obtained with a central injector is shown in Fig. 7(a), where a central region of low Mach number is bounded by higher Mach number regions.

The features of a two-dimensional nozzle flow with a non-uniform flow at nozzle entry were examined using a central injector mounted close to the nozzle entry, as shown in Fig. 11(a), with a 19° nozzle divergence angle. Figure 11(a) displays a schlieren photograph of the flow, together with the pressure distribution on the thrust surface. As discussed in Ref. 31, the expansion wave from the corner of the nozzle interacts with the low Mach number region in the wake formed by the fuel jet, to reflect compression waves back onto the thrust surface, and contribute to the pressure rise seen in the thrust surface pressure distribution at the top of the figure. These expansion interaction compression waves occur together with the compression waves caused by the increase in displacement thickness of the wake due to injection and combustion of the fuel. As these waves pass along flow characteristics, they retain their identity, and may conveniently be identified by their associated flow deflections, as shown by the example in Fig. 11(b). Thus the distribution along the thrust surface of flow deflections which is shown in the figure represents the waves incident on the surface from the expansion interaction, from the increase in wake displacement thickness on the side of the wake nearest the thrust surface, and from the other side of the wake by reflection from the upper nozzle surface. Adding these to obtain the total flow deflection in the waves incident on the thrust surface, and taking the resultant change in the Prandtl-Meyer function (eqn 11) on reflection, the associated pressure increase on reflection of the waves is obtained. This pressure is normalized by the pressure in the nozzle upstream of the compression waves and, as shown by the example in Fig. 11(b), predicts the pressures observed in experiments.

**(Figure 11 here)**

The strength of expansion or compression waves does not change significantly as they pass through the wake. This implies that if the duct entry flow involved multiple wakes, as could occur if there was more than one fuel injection station in the combustion duct, the fact that the waves associated with one of the resultant wakes are able to cross other wakes without altering their strength indicates that, to first order, the wakes may be considered independent of each other for the purpose of determining flow deflection patterns.

Although the aim of these experiments[31] was not to obtain optimum nozzle thrust levels, it is worth noting that the experimental incremental specific impulse corresponding to Fig. 11(b) was a not insignificant 720 sec. With longer combustion ducts than the one employed in these experiments,

better mixing and combustion may be expected to lead to better thrust performance. Because the non-uniformity of the nozzle flow would also be reduced, the present theory would be expected to be particularly applicable to the resulting nozzle flow and may possibly be used as the basis for a means of reducing combustion duct length while retaining near optimum performance. However, it should be added that the wave patterns produced by flow non-uniformity influence the pressure distribution on the thrust surface, and therefore reductions in combustion duct length may be attended by substantial variations in pitching moment.

### 7.5 Three-Dimensional Effects

Although studies of the nozzle flow were centred on the two-dimensional combustion wake produced by a central injector, it was recognized that three-dimensional wakes would result from other injection modes, and that these modes were the ones likely to be preferred in practice. To gain some appreciation of the likely influence of three-dimensional effects in a nozzle expansion, an analysis was undertaken[32] of the expansion of a two-dimensional combustion wake about an expansion corner, with the plane of the wake normal to the corner rather than parallel to it, as in a two-dimensional configuration. An experimental realization of the configuration envisaged would be provided by rotating the central injector of Fig. 8, through 90°, about the axis of the combustion duct. As in the two-dimensional case, the three-dimensional wake-expansion wave interaction produced an increase in thrust, through a pressure increase on part of the thrust surface. Comparison with the analysis of Ref. 31 suggests that the mechanism governing the interaction can be characterized as the tendency of the lower Mach number flow in the wake to deflect more than the mainstream in response to the corner expansion, and the flow changes and the pressure increases at the thrust surface involved in accommodating that tendency.

## 8. THE BUSEMANN SCRAMJET

It is clear that one-dimensional nozzle flow is, so far as sub-orbital scramjets are concerned, an idealization which is useful for assessing the maximum performance that can be delivered with a given nozzle entry flow and area ratio. Where possible, the discussion of the previous section seeks to relate two-dimensional supersonic nozzle flows to one-dimensional flow. However, in general the most accurate and reliable estimate of the thrust delivered by a supersonic nozzle is gained by paying attention to the propagation of waves and their interaction with surfaces. Flow deflection angles and Mach wave angles combine with area change to determine the thrust delivered by a nozzle.

Anticipating that wave phenomena would also have significant effects in operation of a complete scramjet, an heuristic theoretical investigation was made of a simple scramjet configuration[33], consisting of a Busemann biplane with a zone of heat addition at the minimum cross-section, as shown at the top of Fig. 12. The Busemann biplane consists of two thin, double-wedge aerofoils placed to form a duct such that, according to the linearized theory of supersonic flow, the wave drag of the combination can be reduced to zero by suitably choosing the lengths of the surfaces of the duct to match the Mach number of the incoming flow. The biplane is converted into a Busemann scramjet by adding a heat addition zone, which is very short and normal to the flow. This zone is treated as a shock-like discontinuity, with supersonic flow downstream. The duct inlet to minimum area ratio is taken as two and, rather than using linearized theory, the pressure changes across the waves are calculated using supersonic characteristics theory. To obtain the wave paths, the Mach numbers upstream and downstream of the heat addition zone are assumed constant, and the expansion waves in the nozzle are represented as a single wave which follows Mach lines.

**(Figure 12 here)**

Figure 12 shows the effect of waves on thrust and drag with an amount of heat addition of 80% of the heat released by stoichiometric combustion of hydrogen. The curves A and D in the figure

display the variation of nozzle thrust and inlet drag respectively as the precombustion Mach number is varied while altering the lengths of both the nozzle and the inlet to maintain wave patterns which are matched to the nozzle and the inlet. This ensures that no waves escape the duct to produce additional drag. The validity of the assumptions made in calculating the nozzle thrust is confirmed by comparing the curve A for the matched nozzle thrust with the thrust obtained for a one-dimensional nozzle expansion from the post-combustion pressure. Curve B shows the effect of fixing the nozzle configuration so that the nozzle remains matched only for a precombustion Mach number of 6, but allowing the length of the inlet to vary to retain matching. As shown on the right hand side of the figure, waves escape from the duct, thereby increasing the drag and causing curve B to fall below curve A, except at the nozzle matching precombustion Mach number of 6. The curve C shows the effect on inlet related drag of fixing the inlet configuration so that it remains matched only for a precombustion Mach number of 6. In this case waves cannot escape from the inlet, but they propagate through the combustion zone and ultimately are able to escape via the nozzle exit. It can be shown that, in passing through the combustion zone, an incident compression wave produces a transmitted compression wave and a scattered expansion wave, both of which reflect from the surfaces of the nozzle and generate waves which escape from the duct. Curve C is obtained by calculating the total thrust of the nozzle in the presence of the mismatch waves and subtracting the nozzle thrust with a matched inlet and a fixed nozzle (i.e. curve B) in order to obtain the thrust loss, or drag, due to inlet mismatch. This is added to the mismatched inlet drag to produce curve C for the effective inlet drag.

The choice of a precombustion Mach number of 6 for matching of the complete configuration is arbitrary, and similar results would follow if any other high supersonic Mach number were chosen. It can be seen from Fig. 12, that inlet mismatch produces a strong increase in effective drag as the Mach number increases above 6, and when this drag is subtracted from the reduced thrust due to nozzle mismatch (i.e. curve B) no significant net thrust remains at a precombustion Mach number of 8. On the other hand, the effect of reducing the precombustion Mach number below 6 is not so serious. For example, the difference between curves B and C at a precombustion Mach number of 4 yields a net thrust which is 75% of the matched inlet and nozzle thrust. This suggests that, if a scramjet is to operate with changing Mach numbers, then it is best to design for the maximum Mach number.

Two simplifications, which were made to facilitate analysis, are worth some further comment. First, because the analysis is limited to a duct contraction ratio of two, the associated performance of the scramjet is also limited. Thus the difference between thrust and drag at a precombustion Mach number of 6 in Fig. 12 would amount to an approximate specific impulse of only 400 sec for hydrogen fuel. Of course, a larger contraction ratio and a better performance would be obtained by adding to the length of the inlet and nozzle in such a manner that the resultant inlet and nozzle would still be matched at a precombustion Mach number of 6. This would lead to a more complicated analysis, but one which may be expected to yield results displaying the same trend as those shown in Fig. 12.

Second, the heat addition will take place over some finite length of combustion duct, rather than the infinitely thin zone which has been assumed. However, propagation of waves through the combustion duct will still take place, together with the generation of secondary waves. Thus an effective inlet drag, similar to curve C, can be expected to arise from inlet mismatch with a finite length combustion duct.

## 9. FORCE MEASUREMENT

Although the research on the combustion duct and thrust nozzle was less than exhaustive, it was considered sufficient to proceed to the next stage, which was to experiment with complete scramjet configurations. These involved the integration of the inlet, combustion duct and thrust nozzle into

one complete model. The obvious measurement to initially make on such models is the net thrust (or drag) as this is the essential measure of installed scramjet performance. Such measurement demanded the development of a new shock tunnel measurement technique.

The need for such a technique as made evident by the experimental results obtained in the combustion duct and nozzle studies. These results made it clear that integrated models could be expected to be of a size such that the flow traverses only a few model lengths during the test time. This would be particularly true for slender models envisaged for integrated scramjet experiments. Now, when the shock tunnel flow is initiated and forces are rapidly applied to the model, stress waves will occur in the model which will, by reflection and re-reflection, traverse the length of the model many times before the model comes into stress equilibrium. It follows that the few flow model lengths of test time available in a sub-orbital shock tunnel were, in general, not sufficient for the model to come into stress equilibrium, and therefore that the overall forces acting on a model could not be measured by available force balance methods, since these treated the model as a rigid body.

Fortunately, the stress waves which were the source of this difficulty could themselves be exploited to measure the force on the model, by placing strain gauges on the model support system, and recording the time history of the strain produced by the stress waves passing into the supports. Deconvolution of the strain records then would yield the forces on the model. For measurement of the thrust or drag of a slender body, supported from a downstream sting, a single strain gauge, recording the strain time history of stress waves passing into the sting, would yield a satisfactory measurement.

The relation between the strain measured in the sting, $y(t)$, and the axial force on the model $u(t)$, can be described by the integral

$$y(t) = \int_o^t G(t-\tau)\, u(\tau)\, d\tau, \qquad (12)$$

where $G(t)$ is a pre-determined impulse response function, and $t$ and $\tau$ are time. The impulse response function can be determined numerically or by experiment – for example, by measuring the strain history resulting from application of a sudden increase in axial load on the model. The deconvolution of the integral of eqn (12) to yield the axial force history, $u(t)$, from the recorded strain history, $y(t)$, is accomplished by a numerical procedure using a personal computer.

The method was first applied to measurement of the drag on a relatively short cone, with 15° semi-vertex angle[34]. In this case the internal stress waves in the model were unimportant, but the stress wave balance was established as a viable method of measuring axial force. Subsequent measurements of drag were made on a 5° semi-vertex angle cone 425 mm long[35, 36], where the internal stress wave reflections were significant, and yielded results consistent with theoretical estimates. The sensitivity of the method to the distribution of drag producing forces on the model was investigated numerically during this project leading to the conclusion that measured drag was independent of the force distribution on the cone.

The numerical investigations just referred to included a case where the drag force was concentrated at the tip of the cone. The fact that this did not influence the measured drag was exploited to conduct an investigation of the effect of nose blunting on the drag of a 5° semi-vertex angle cone[37]. The tests were done at a stagnation enthalpy of 15 MJ/kg with a test flow in which driver gas contamination occurred, but was less than 30% of the test flow by molar concentration. It was found that the drag remained at a constant value when the radius of the blunt nose remained less that 0.12 times the radius of the base of the cone. This indicates that a moderate degree of nose

blunting could be used to accommodate nose tip heat transfer effects on scramjet intakes without directly affecting the drag.

The stress wave force balance has also been used with a two-dimensional straight thrust nozzle in an exercise aimed at determining the influence of skin friction on thrust[36]. The nozzle had plane sidewalls, was 300 mm long and 54 mm wide, and had two thrust surfaces which were symmetrically disposed about the nozzle centreline, each with a divergence angle of 11°. The nozzle was supported by a two sting system, and was otherwise freely suspended immediately downstream of a fixed combustion duct, which supplied flow to the nozzle. Provision was made for fitting the thrust surfaces with transducers. Thus the measured net thrust could be compared with the thrust obtained from measured pressure distributions to assess the thrust loss due to skin friction. It was found that this thrust loss was 20% ± 5% of the pressure thrust, and was consistent with approximate estimates using a skin friction co-efficient of $3 \times 10^{-3}$. These estimates indicated that approximately half of the skin friction drag was associated with the nozzle walls, and therefore the skin friction drag on the thrust surfaces was roughly 10% of the pressure thrust. However, the presence of combustion in the combustion duct did not measurably affect the skin friction drag, indicating that the combustion thrust increment, obtained by subtracting the fuel-off pressure thrust from the fuel-on pressure thrust, is not measurably affected by skin friction.

The stress wave balance method was extended to simultaneously measure three components of force[38], and was used for experimental measurement of the lift, drag and pitching moment on a 15° semi-vertex angle cone, 220 mm long, at angles of incidence which varied from 0° to 5°. Results were consistent with theoretical calculations, and led to use of the three component stress wave balance for scramjet experiments, as described below.

Finally, measurements of drag have also been accomplished by a stress wave force balance in the 50 microsecond test time of a small expansion tube[39]. The drag of a series of cones, with a base diameter of 16 mm and semi-vertex angles ranging from 20° to 45°, was measured in a carbon dioxide flow, at a velocity of 7.5 km/s, and yielded results which were consistent with theory. This was a significant development, as it implied that this method of measuring model forces could be applied to impulse facilities in general, particularly those with shorter test times than a shock tunnel. In conventional wind tunnels experience indicates that some two thirds of wind tunnel tests are devoted to force measurement, because of its importance to performance. The development of the stress wave force balance introduces the possibility of routine performance evaluation to impulse facilities, and therefore may be seen as a major extension of impulse facility capability.

## 10. INTEGRATED SCRAMJET FORCE MEASUREMENTS

With the development of the stress wave balance for measuring axial force it became possible to measure the thrust/drag performance of integrated scramjet configurations. At the time that a scramjet configuration was selected for such experiments, experience with the stress wave force balance had largely been restricted to axisymmetric configurations, and therefore the axisymmetric scramjet model, shown in Fig. 13(a), was chosen for the experiments[40]. The model is shown with half the cowl removed. It consists of an axisymmetric centrebody, with six combustion chambers and associated intakes arranged about its periphery. These intakes consist of compression ramps formed by the splitters which separate the combustion chambers.

**(Figure 13 here)**

### 10.1 Model Design

As pointed out in the introduction, experiments with integrated scramjet configurations are more demanding of shock tunnel performance than the component experiments described so far. This is illustrated in the design of the scramjet model.

In order to avoid the possibility of thermal choking at the lower end of the sub-orbital velocity range, a design post combustion Mach number of approximately 2 was chosen which, with a constant area combustion duct and a heat release corresponding to stoichiometric combustion of hydrogen, implied a precombustion Mach number of approximately 4. This Mach number is a result of the inlet compression process. For a scramjet in atmospheric flight, where the static temperature is fixed, it would be necessary for the inlet compression process to yield precombustion temperatures and pressures which are high enough to assure ignition and burning of the fuel but, because the shock tunnel can supply an airflow at any reasonable freestream temperature, the temperature requirement can be relaxed. The function of the scramjet inlet compression process in a shock tunnel is therefore to raise the precombustion pressure to a suitable multiple of the freestream pressure. Choosing a value of 10 for this multiple, representing a reasonable thermal cycle efficiency, and an inlet compression process which took place through three oblique shocks, resulted in a freestream Mach number of 6 and an inlet contraction ratio of 4.8. Detailed intake considerations reduced the inlet contraction ratio to 4.4. The thrust nozzle expansion ratio is, through geometrical considerations, related to the inlet contraction ratio and, with the value of the inlet contraction ratio just quoted, the expansion ratio of the thrust nozzle was 5.8. Referring to Fig. 7(c), this expansion ratio was in the region where a large part of the potential thrust, which could be produced by the nozzle expansion, had been achieved, and further significant increases in thrust would demand large increases in nozzle area ratio.

The value of the precombustion pressure must be sufficient for the combustion reaction and associated heat release to take place. For the hydrogen-air reaction, Fig. 6 indicates that the value of the product of precombustion pressure and combustion chamber length should be approximately 15 kPa m. The length of the combustion chamber, at 0.06 m, was limited by the model size, which was itself limited by the shock tunnel test time, and this combustion chamber length led to a required precombustion pressure of 250 kPa. Unfortunately, the shock tunnel nozzle supply pressure was limited to 40 MPa for these experiments and, with a freestream Mach number of 6, the precombustion pressure was limited to 100 kPa. Thus the limitation of the shock tunnel nozzle supply pressure led to a precombustion pressure which was insufficient to sustain complete hydrogen-air combustion. Or, to put it another way, the demands made by this integrated scramjet experiment exceeded the shock tunnel performance levels.

However, by using hydrogen fuel mixed with silane ($SiH_4$), as an ignition promoter, it was possible to reduce the pressure required for combustion. The results of central injector constant area combustion duct experiments with hydrogen-silane fuel mixtures[41] indicated that, at the expected minimum scramjet model precombustion temperature, of 800 K, the required value of the product of precombustion pressure and combustion chamber length was approximately 3kPa.m with a fuel mixture which included between 20% and 5% of silane by molar concentration. Assuming that, as with hydrogen fuel, the mode of injection would not significantly affect the combustion lengths, it was concluded that a fuel consisting of 13% silane and 87% hydrogen would undergo complete combustion heat release within the combustion changer length at a precombustion pressure of 100 kPa.

Relatively large increases in pressure occur through the inlet compression process, and the boundary layers must be able to negotiate these pressure increases without separating. Therefore the Reynolds numbers on the forecone of the model should be high enough to ensure transition to a turbulent boundary layer. A study of transition on a flat plate in the shock tunnel[42] had yielded a transition Reynolds number which varied from $2.5 \times 10^6$ to $1.0 \times 10^6$ as the stagnation enthalpy increased. The corresponding forecone Reynolds numbers were $2.7 \times 10^6$ to $1.2 \times 10^6$ over the same range of stagnation enthalpies and this, together with the disturbances to the boundary layer

generated by the compressions shocks, indicated that transition to a turbulent boundary layer would occur on the forecone.

Figure 13(b) shows the scramjet model in operation in the shock tunnel. Flow luminosity on the forecone arises from flow compression by the conical shock formed on the forecone. The absence of the regions of high luminosity which would be associated with the strong shock waves resulting from choking is an indication that the inlet compression process is performing as designed. The high luminosity seen at the downstream end of the cowl is associated with the combustion region, and is thought to be due to silicon released during the combustion process.

10.2 Performance of the Model

The performance of the scramjet model in shock tunnel tests is presented in Fig. 14 in terms of the net thrust coefficient $C_{TN}$. Two continuous lines are displayed, with associated experimental points, showing the comparison between experimental and theoretical values of the axial force, both with fuel injection and without fuel injection. The theoretical values were obtained by adding the calculated inviscid and viscous axial forces acting on the inlet, the combustion chambers and the thrust nozzle. The consistency between the axial forces calculated in this manner and the measurements served as a check on the validity of the calculation. Figure 14 also displays two broken lines. The lower one on the figure represents the fuel off drag, and is fitted by eye to the associated experimental points. This broken line was used to yield values of the drag coefficient, $C_D$, for the upper broken line, which was obtained from a third version of the net thrust equation, written as

$$C_{TN} = 2ne_n\left(\Delta Q/U^2\right)\left(1-0.5\Delta Q/U^2\right) - C_D + C_j \qquad (13)$$

Equation (13) is derived from eqn (9), the second version of the net thrust equation, by adding $C_j$, the thrust coefficient derived from the reaction thrust generated by fuel injection, and by incorporating the factor $e_n$ in the first term on the right hand side of the equation to account for the efficiency of the thrust nozzle. This efficiency is the ratio of the thrust developed by the nozzle (which was calculated by using a simplified three-dimensional method of characteristics analysis) to the thrust which would be developed by one-dimensional flow in a nozzle of the same area ratio. The drag coefficient, $C_D$, is obtained by combining the fuel off drag coefficient with a small contribution, due to fuel on increases in the viscous drag of the combustors, which ranged from 0.026 to 0.008 as the stagnation enthalpy increased from 3 MJ/kg to 8 MJ/kg. Equation (13) yields values of the net thrust coefficient which are generally consistent with the experimental results, with a tendency to somewhat underpredict the drag at stagnation enthalpies exceeding 4 MJ/kg. A positive thrust was obtained only at stagnation enthalpies below this level.

**(Figure 14 here)**

At stagnation enthalpies below 3.0 MJ/kg, unsteadiness in the thrust began to appear, and attempts to increase the thrust, either by further lowering the stagnation enthalpy or by increasing the fuel equivalence ratio, led to choking of the scramjet inlet. This is unlikely to have been due to thermal choking of the combustion chambers, as eqn (2) indicates that insufficient heat release is taking place. However, if the Mach number after the shock at the tip of the conical forebody (i.e. where the boundary layer originates) is used in the separation criterion of eqns (3), the predicted pressure for the onset of separation is close to the pressure obtained after combustion, indicating that choking was due to boundary layer separation. Of course, this implies that the pressure rise to boundary layer separation is unaffected when the pressure rise takes place through a number of stages, as in this case.

Equation (13) provides a reasonable estimate of the performance of a scramjet as it penetrates the sub-orbital regime, and serves to reveal the relative magnitude of the phenomena governing performance, through the terms on the right hand side of the equation. The heat release, in the first term, was determined by assuming that the fuel mixture of 13% silane and 87% hydrogen burned completely to produce $H_2O$ and $SiO_2$ and therefore, at the fuel equivalence ratio of 0.77 used in the experiments, provided a heat release in air of 2.3 MJ/kg. Pressure measurements in the combustion chamber displayed a pressure rise consistent with this value of heat release. A value of $n$ of 0.33 was used which, referring to Fig. 7, was appropriate to a thrust nozzle area ratio of 5.8, and the value of $e_n$ was calculated to vary from 0.81 to 0.62 as the stagnation enthalpy varied from 3 MJ/kg to 8MJ/kg. Thus, over this stagnation enthalpy range, the magnitude of the heat release term varied from 0.181 to 0.062. It is worth noting that these values do not represent a universal maxima for this term. For example, if the heat release was 3.4 MJ/kg, corresponding to hydrogen fuel at an equivalence ratio of one, and a perfectly efficient nozzle of area ratio 20 could be designed, yielding a value of $2ne_n$ of 0.9, then the magnitude of this term would range from 0.39 to 0.21 over the same stagnation enthalpy range. The thrust coefficient given by eqn (13) would then approach zero only as the stagnation enthalpy approached 9 MJ/kg. Clearly, substantial gains in performance can be obtained by attention to the efficiency of heat release in combustion and the thrust nozzle design.

The fuel injection thrust coefficient, $C_j$, ranges in value from 0.043 to 0.029 as the stagnation enthalpy varies from 3 MJ/kg to 9 MJ/kg and therefore, as expected, makes only a moderate contribution to the net thrust. Thus the drag coefficient term, $C_D$, which is dominated by the measured fuel off drag, plays a major part in determining the net thrust or drag. The inviscid component of the fuel off drag varies from 60% to 50% of the total fuel off drag as the stagnation enthalpy increases from 3 MJ/kg to 8 MJ/kg. This component arose primarily from the inlet and cowl drag. At an intermediate stagnation enthalpy, of 5.5 MJ/kg, the thrust nozzle reduced the drag by 20% but, if a one-dimensional nozzle flow were achieved, this drag reduction would rise to 30%. The cowl contributed 25% of the inlet and cowl drag, and the entropy rise across the inlet shocks contributed approximately 20% to the inlet drag. These losses account for almost all the inviscid drag, and are all susceptible to reduction by better design.

The viscous drag accounts for approximately half of the total fuel off drag, and is roughly equally divided between the inlet viscous drag and the drag of the combustion chambers. The inlet boundary layer was expected to be predominantly laminar, while the combustion chambers and thrust nozzle boundary layers were expected to be turbulent. As foreshadowed in Section 9, viscous drag in the thrust nozzle made only a small contribution to the drag. As an illustration of the importance of viscous drag, it is noted that if halving of the viscous drag could accompany halving of the inviscid drag then, for the example using hydrogen fuel in the above paragraph but one, the stagnation enthalpy at which the net thrust coefficient of eqn (13) would approach zero would be raised from 9 MJ/kg to 15 MJ/kg. The viscous drag component is likely to become even more important with increasing penetration into the sub-orbital regime. As indicated in Section 8, it is desirable to design a scramjet vehicle for a Mach number close to its maximum operating value, and this will involve increasingly slender configurations as the maximum Mach number increases, which will be subject to increasing viscous drag.

### 10.3 Hydrogen Fuelled Scramjet Models

The use of a silane-hydrogen mixture as fuel did indeed reduce the value of the pressure × combustion chamber length parameter required for essentially complete combustion, but it also increased the mixture molecular weight with respect to hydrogen, and therefore had the disadvantage that it reduced the fuel specific impulse. In an attempt to show experimentally that this reduction could be avoided, a scramjet model was designed in which combustion of hydrogen fuel would be encouraged, without the need for an ignition promoter[43]. Figure 15 shows detail of

one half of the model, which was symmetrical about the plane AA' in the figure. This symmetry was necessary because, at the time the experiments were done, the force balance could only operate with axial loads. An inlet contraction ratio of 5.2 was used, with the aim of producing a local region of high temperature and pressure and, to minimize choking tendencies when combustion occurred, was followed by a divergent combustion chamber. Hydrogen fuel injection took place at the minimum cross-section. It was found that, although the model flow started and ran during the shock tunnel test time with no fuel injection, the flow choked when the fuel flow was initiated before the shock tunnel flow, but ran when the fuel flow was initiated after initiation of the shock tunnel flow. A possible explanation for the choking effect may be that the injected fuel interacted with the shock tunnel nozzle starting flow to establish a choked flow which was subsequently maintained by combustion. Using the delayed fuel injection technique, it was possible to establish a steady flow with hydrogen combustion.

**(Figure 15 here)**

In experiments at a stagnation enthalpy of 3.5 MJ/kg and a Mach number of 6.4, the thrust with combustion increased with equivalence ratio, and became equal to the drag as the equivalence ratio approached unity, thus achieving the cruise condition of net zero thrust or drag. By comparison with results of pressure measurements in a combustion duct-thrust nozzle combination, it was concluded that combustion was taking place in the thrust nozzle[29, 43] but, as indicated by a measured fuel specific impulse of 835 sec, a portion of the fuel did not burn. Thus, although the use of an ignition promoter had been avoided, the fuel specific impulse of hydrogen fuel had not been fully realised. It is worth noting that the fuel off drag coefficient was 0.183, which is similar to the drag coefficient of the axisymmetric scramjet model discussed above, and was again divided approximately equally between inviscid and viscous drag.

10.4 Lift and Pitching Moment on a Scramjet Model

While experiments with the stress wave force balance were initially limited to the measurement of axial force on scramjet models, continued development of the balance technique made it possible to measure the lift and pitching moment on a scramjet model, as well as the axial force[44]. A simple two-dimensional model configuration was chosen, as shown in Fig. 16(a), consisting of an inlet ramp, a combustion chamber and a two ramp thrust nozzle. The inlet contraction ratio was 4.0, and 3 mm thick sideplates were fitted to ensure a two dimensional flow path. The model, which is shown in a streamwise sectioning plane in the figure, was supported by four stress bars and, by recording the timewise variation of strain on those bars, followed by subsequent devolution of that record, the lift and pitching moment during a test, as well as the axial force, could be obtained[44]. The stress bars and the upper surface of the model were enclosed in a shroud which protected them from the test flow, and therefore the forces acting on the model did not include the skin friction drag on the upper surface, which would be present if a free flying model was used. Hydrogen fuel was injected on the inlet ramp, at 45° to the airflow direction, from orifices stationed at 58% of the distance from the leading edge to the beginning of the combustion duct.

**(Figure 16 here)**

The variation of the lift and the pitching moment are shown in Figs. 16(b) and 16(c) as the equivalence ratio was varied at a stagnation enthalpy of 3.3 MJ/kg and a Mach number of 6.5. The lift increases linearly with equivalence ratio, until the equivalence ratio exceeds unity. Comparison with results when hydrogen was injected into nitrogen test gas confirm that the increase was due to combustion. The combustion pressure increase in the combustion duct is not expected to make a substantial contribution to the lift because the pressures on the interior of the cowl will largely cancel the lifting effect of the pressures on the body surface. Therefore the observed combustion induced lift increment was primarily due to changes in the thrust surface pressures. As discussed in

sub-section 7.4, the thrust surface distribution of pressure can be expected to change as the combustion wake changes, and therefore it comes as no surprise that, as shown in Fig. 16(c), there are substantial variations in pitching moment as the equivalence ratio increases. Since a positive value in the figure signifies a nose-up pitching moment, the pitching moment variations shown translate into a nose-down centre of pressure shift of 5% of the model length as the equivalence ratio changes from zero to one when nitrogen gas is used, and a nose-down centre of pressure shift of 11% of the model length when the use of air test gas allows combustion to take place. Thus, combustion can cause large shifts in the centre of pressure for scramjets.

The measured net axial force was negative, signifying net drag, and increased with equivalence ratio to approach zero at an equivalence ratio of 1.4. This suggested that somewhat less than complete combustion occurred, an interpretation which is consistent with the value of 11 kPa.m for the product of the precombustion pressure and the combustion duct length. Comparing this value with the value of 15 kPa.m necessary for complete combustion in Fig. 6, and noting that, because the precombustion temperature of 900 K was somewhat less than the lowest value of Fig. 6, combustion lengths would have increased, it is apparent that the length of the combustion duct was insufficient for complete combustion. This conclusion was reinforced by the measurement of relatively low values of fuel specific impulse. For example, a fuel specific impulse of 650 sec was measured at an equivalence ratio of one.

It is worth noting that, once again, the fuel off drag was equally divided between inviscid and viscous components.

10.5 Boundary Layer Separation and Choking

Experiments carried out at a stagnation enthalpy of 2.8 MJ/kg and a Mach number of 6.6, with a scramjet configuration involving a boundary layer dump immediately upstream of the combustion duct[45] indicated that the separation criterion of eqn (3a) provided a good prediction of the occurrence of choking. The boundary layer dump caused a new boundary layer to start at the entrance to the combustion duct, thus avoiding the complication introduced by processing the boundary layer through the inlet compression. These experiments confirmed that the two-dimensional criterion due to Korkegi would apply to a nominally three-dimensional situation.

However, for both the axisymmetric scramjet model of sub-section 10.2, and the hypersonic cruise scramjet model of sub-section 10.3, the application of the criteria of eqns (3) to the combustion duct alone failed to predict the choking which did occur, whereas separation and choking was predicted in each case if the criteria were applied with the boundary layer originating at the model leading edge. Thus, even when the boundary layer is required to negotiate the pressure rise due to inlet compression and the combustion induced pressure rise as well, eqns (3) appear to remain useful for predicting separation and choking, at least at stagnation enthalpies around 3.0 MJ/kg and test flow Mach numbers around 6.5.

Of course, it is desirable to test this separation and choking criterion over a range of velocities and Mach numbers but, accepting its validity, it introduces yet another factor to be accommodated in designing an integrated scramjet model. It is clear that increasing the inlet contraction ratio can have considerable benefits in increasing the combustion duct pressure, thereby reducing the length needed for complete combustion, and also in increasing the thrust nozzle area ratio, thereby generating more thrust. Unfortunately, these benefits are denied by the limit on overall pressure rise imposed by eqns (3).

Thus, raising the operating pressure levels of the shock tunnel in order to raise the test flow supply pressure would, at the same Mach number, raise the precombustion pressure in the combustion duct, and this would bring the hydrogen fuelled scramjet models of sub-sections 10.3 and 10.4

closer to complete combustion, which can be expected to increase the net thrust. However, gains in the net thrust which would follow from increases in the test section Mach number allowed by an increased nozzle supply pressure would be limited (except with the use of an ignition promoter) since the fall in test section static pressure occasioned by an increased test section Mach number would tend to outweigh allowable gains in this inlet contraction ratio permitted by eqns (3).

## 11. INLET INJECTION, RADICAL FARMING AND KINETIC AFTERBURNING

The integrated scramjet force measurements indicated that mixing and combustion of hydrogen could not be completed at the precombustion pressures and combustion duct lengths of these experiments. Not only did this limitation lead to development of the shock tunnel to increase operating pressure levels, but it also encouraged experiments on two concepts – one designed to reduce combustion duct lengths for complete combustion, and the other to explore a mode of combustion different from the diffusion flame modes considered so far.

The first of these concepts involved injection of fuel on the inlet. This has already been mentioned in connection with the experiments of sub-section 10.4, and was studied in more detail in Ref. 46. Inlet injection has clear advantages in allowing mixing of hydrogen with air at the relatively low temperatures of the inlet before the mixture enters the combustion duct and ignites, thereby ensuring that the combustion process in the combustion duct is not delayed by the necessity for mixing. However, it was important to ensure that ignition did not occur prematurely, and thereby cause drag on the inlet due to the resulting combustion pressure increase. Experiments involving surface pressure measurements and shadowgraph flow visualization were done with injection through surface orifices in the inlet. The scramjet walls were at room temperature and the stagnation enthalpy was 3.0 MJ/kg[46]. No evidence of inlet combustion was detected, but combustion was observed in the combustion duct. Experiments were also done with hydrogen injected through orifices in an inlet surface which was heated to a temperature of 500 K[47], and no evidence of inlet combustion was detected either by surface pressure measurements or by interferometric imaging.

The second concept combined inlet injection with a technique to promote early ignition of the fuel-air mixture called "radical farming"[48]. This technique is illustrated in Fig. 17(a), which represents a two-dimensional scramjet configuration. The shocks or compression waves which make up the inlet compression process are arranged to form a local region of elevated pressure and temperature, near the entrance to the combustion duct, where the production of the chemical radicals, which are a first stage in the overall combustion process, will be encouraged. This region is called the radical farm, and is isolated from the walls of the combustion duct by a lower pressure, cooler flow. The radical farm is terminated by the expansion waves from the corner at the combustion duct entrance, but the radicals remain "frozen" in the flow until they meet another region of elevated temperature and pressure, where the combustion process continues. The benefit of radical farming is that, because of the exponential dependence on temperature of the rate of radical formation, the regions of elevated temperature and pressure in the radical farms provide accelerated development of the ignition process.

**(Figure 17 here)**

Experiments were done with the two-dimensional configuration of Fig. 17(a). The model was 75 mm wide, and was fitted with sideplates to ensure two-dimensional flow. Pressure measurements were taken, in the model midplane, along the inlet, combustion duct and thrust nozzle, together with measurements along three transverse lines to check that the flow was two-dimensional. Typical pressure distributions are displayed in Fig. 17(b), and show that vigorous combustion occurred within the length of the combustion duct. Using the inlet flow conditions, a mean precombustion temperature of 700 K is obtained for the case of Fig. 17(b), a temperature which has been found to be too low for combustion in other experiments with constant area combustion ducts. Thus radical

farming offers considerable improvement in the ignition characteristics of a hydrogen fuelled scramjet.

Integration of the measured pressure distributions was used to obtain a two-dimensional inlet drag and nozzle thrust, and this was combined with skin friction calculations for all interior surfaces (including the interior of the sideplates) to obtain an interior flow path net thrust. Using measured values of the injected fuel mass flow, this net thrust could be converted to a net specific impulse, which is presented in Fig. 17(c). The inlet contraction ratio was varied by adjusting the separation between the upper and lower halves of the scramjet model, as shown in Fig. 17(a), and at each contraction ratio, the equivalence ratio was increased until choking occurred. At a stagnation enthalpy of 3 MJ/kg, the equivalence ratio for choking fell from 0.65 to 0.35 as the contraction ratio was increased from 2.9 to 4.1, and at 4 MJ/kg, it fell from 0.85 to 0.40. Estimates indicated that, as the contraction ratio changed, the radical farms persisted without major changes in their dimensions, suggesting that combustion processes in the model were essentially independent of the contraction ratio. This is in contrast to the more conventional scramjet, where the inlet contraction ratio determines the precombustion temperature, which strongly influences the combustion process. Figure 17(c) confirms this independence by presenting points which are obtained by taking the mean of two to four measurements of the net specific impulse near the choking limit at each value of the contraction ratio. As represented by the cross-hatched zones, the net specific impulse values tended to remain constant as the contraction ratio was varied at both of the stagnation enthalpies tested, indicating that combustion heat release was not significantly affected by the changes in contraction ratio. It may also be observed that the net specific impulse values, though small, are all positive indicating that positive net thrust was obtained for the internal flowpath of this scramjet model.

It is also worth noting that eqns (3) again predicted approximate separation and choking limits based on the Mach number at the leading edge.

A third concept offers a method of partly circumventing the limitation arising from boundary layer separation induced choking. The method is called "kinetic afterburning"[29], and involves the use of the combustion duct to produce the free radicals which precede the heat release reactions, while those reactions are delayed until the flow enters the thrust nozzle. Thus the pressure increase due to combustion takes place after the flow has experienced some expansion, and the boundary layer is only required to negotiate an overall increase in pressure which is less than that arising from the inlet compression followed immediately by the combustion pressure rise. The experiments of Ref. 29 indicate that kinetic afterburning can be effected without excessive loss of thrust, suggesting that it may be useful as a means of allowing a scramjet with a fixed inlet contraction ratio to extend its operating range to lower Mach numbers without choking.

These three concepts have the common purpose of reducing the effect of limitations on the combustion process which became evident through the experiments of Section 10. Inlet fuel injection and radical farming may be expected to produce more complete combustion in shorter combustion ducts, and kinetic afterburning can be expected to bypass the choking effect of the combustion pressure increases. All await evaluation, in terms of their effect on the net thrust equation, through force balance measurements.

## 12. SKIN FRICTION MEASUREMENT

The measurements on integrated scramjet models indicated that further penetration into the sub-orbital regime was hindered by a number of factors, apart from the need for full combustion heat release. Referring to eqn (13), the net thrust equation, and Fig. 14, it is clear that the fuel off drag plays a major role as one of these factors, and analysis indicates that half of this drag is due to skin friction. In principle, the other half of the drag, which is due to inviscid flow effects, can be

usefully studied by analytical or numerical means but, because the flow conditions associated with combustion ensure that turbulent boundary layers prevail, a predominantly experimental approach was taken for the study of skin friction.

12.1 Skin-Friction Gauge Development

For operation in the shock tunnel T4, it was desirable to have a skin friction gauge with a resonant frequency higher than 10 kHz. Therefore a floating element design was chosen in which the measuring element was a piezoelectric disc, and the floating element was a thin metal disc, which was mounted to be flush with the surface on which skin friction was to be measured, and was bonded directly to the piezoelectric disc. Early experiments[49] indicated that a satisfactory gauge response time could be obtained with this design, and it was used to experimentally confirm the value of Reynolds analogy factor in a high enthalpy laminar boundary layer[50]. Further development resulted in the skin-friction gauge illustrated in Fig. 18(a)[51]. On the left side of the figure is a schematic representation of the operation of the gauge, with the direction of polarization of the piezoceramic (PZT-5H™) disc either parallel or anti-parallel to the direction of the shear force to be measured. The right side of the figure shows the gauge assembly, with the measuring piezoceramic mounted on a rigid base, and the acceleration compensating piezoceramic and dummy floating element mounted in a manner such that its response to spurious vibration and acceleration of the gauge could be used to cancel the response of the measuring piezoceramic, to leave an output which measured the shear force applied to the floating element. Vibration and acceleration of the gauge was minimized by mounting the gauge on felt washers, which involved adjusting the washers after each shock tunnel test.

**(Figure 18 here)**

The lowest natural frequency of the gauge was 40 kHz, which allowed it to follow the development of the shock tunnel flow. The inset in Fig. 18(b) shows the development of the measured skin friction in a zero pressure gradient turbulent boundary layer in comparison with the development of the local static pressure. The skin friction gauge follows the static pressure with only a slight delay, reflecting the expected lag behind the pressure as the boundary layer reaches a steady state.

The gauge was used in an investigation of zero pressure gradient turbulent boundary layers on one wall of a rectangular duct 1.5 m long at stagnation enthalpies up to 12 MJ/kg[52], and the variation of measured skin friction with Reynolds number, at a stagnation enthalpy of 6.5 MJ/kg, is shown in Fig. 18 (b). The measurements are consistent with a number of theoretical correlations, and follow thin film gauge heat transfer measurements in locating the range of Reynolds numbers over which transition occurs. Figure 18(b) is typical of results obtained across the range of stagnation enthalpies investigated, and indicate that the analytic models used to describe hypersonic turbulent boundary layers may be used in the sub-orbital regime, at least up to velocities of 5 km/s. However, a possible exception to this is the observation made during this investigation that, in contrast to the trends observed by other investigators in the hypersonic regime, the Reynolds analogy factor decreased from 1.25 to 0.7 as the skin friction coefficient increased from $10^{-3}$ to 3 x $10^{-3}$.

12.2 Skin Friction with Mainstream Combustion

Calculations indicate that, of the half of the fuel-off drag due to skin friction, approximately half is due to skin friction in the combustion duct. This is not surprising, since the flow density is a maximum in the combustion duct and this translates into a maximum in the skin friction. Although it was assumed that the skin friction with mainstream combustion could be predicted using existing theories, incorporating the mainstream changes brought about by combustion, there was a need to confirm this by experiment at suborbital stagnation enthalpies.

Therefore skin friction measurements were made in a rectangular combustion duct, of 48 x 100 mm cross section, with a central injector[53]. The injection strut was in the midplane of the duct, spanning the 100 mm dimension, and the wall on which the measurements were made was parallel to the injection plane, to yield a flow which was essentially two dimensional. The boundary layer was turbulent and stagnation enthalpies of 5.7 MJ/kg and 6.8 MJ/kg were investigated. Unfortunately, flow disturbances originating in the combustion wake were evident in the skin friction measurements, and this reduced the accuracy of those measurements. Nevertheless, taking the mean of a number of tests at each of three measuring stations indicated that the mean fuel-on skin friction differed from the mean fuel-off skin friction by an amount that varied in the range of +30% to -10% of the fuel-off skin friction. Since the fuel-off measurements were consistent with existing theory, so were the fuel-on measurements, at least within the accuracy noted.

Measurements of the skin friction drag on a circular combustion duct were also made by using the stress wave force balance technique[54]. These experiments had the twofold aim of determining the effect of crossflow injection of fuel on the skin friction, and of improving on the accuracy achieved in the experiments of the previous paragraph. By measuring the skin friction drag integrated over the length of the combustion duct, the effect of local flow disturbances radiated from the combustion wake would be averaged out. Figure 19(a) shows a half section of the experimental model. The combustion duct was 33 mm in diameter with a pressure measuring manifold and an O-ring seal at each end. Hydrogen fuel was injected normal to the flow from five injection ports, equally spaced about the circumference, 24 mm upstream of the leading edge of the combustion duct. The duct was attached to the stress wave bar, as shown, and shrouds enclosed the complete assembly to ensure that only the force on the inner surface of the combustion duct was measured. Apart from a correction of less than 10% arising from the pressure at the ends of the duct, this measured force was the skin friction drag on the combustion duct.

**(Figure 19 here)**

Skin friction drag measurements were carried out with turbulent boundary layers at a stagnation enthalpy of 7.2 MJ/kg, using ducts of varying length. The results are displayed in Fig. 19(b). The extraneous force noted in the figure was due to a leak at one end of the duct, which was detected and calibrated during the experiments. Taking this into account, the experimental results indicated that there was no measurable difference between the fuel-on and fuel-off measurements of skin friction, and both were consistent with existing theory for turbulent boundary layers.

The experiments of this sub-section were conducted at stagnation enthalpies high enough to avoid choking, but low enough to yield substantial combustion induced changes in the mainstream flow. Existing theory, using these combustion induced changes, does not predict changes in skin friction which are large enough to be detected at these stagnation enthalpies. However, it should be noted that at lower stagnation enthalpies greater combustion induced changes in skin friction are predicted, and these changes have been incorporated in the successful predictions of net thrust in sub-section 10.2.

### 12.3 Skin Friction Reduction by Boundary Layer Combustion

The importance of skin friction drag in reducing the net thrust with an integrated scramjet configuration focussed attention on a means of reducing skin friction in turbulent boundary layers. Noting that the Reynolds stresses in a turbulent boundary layer play the role of viscosity, and that they are density dependent, it was thought that they could be reduced by raising the temperature, thus reducing the effective viscosity. In addition, the reduction in density would increase the width of the boundary layer streamtubes, and these two effects of increasing the boundary layer temperatures would both tend to reduce the skin friction.

This concept was tested by doing experiments with the rectangular duct configuration shown in Fig. 20(a)[55] at a stagnation enthalpy of 7.8 MJ/kg and a pre-injection pressure, temperature and Mach number of 50 kPa, 1500 K and 4.5 respectively. Hydrogen was injected from a room temperature reservoir, at a Mach number of 1.8, through a slot at the wall which spanned the 100 mm dimension of the duct cross-section. Thus the flow over the surface downstream of the slot was nominally two dimensional. As shown in the figure, this surface was instrumented to measure pressure and heat transfer, while four of the skin friction gauges described in sub-section 12.1 were used to measure skin friction at the indicated station. The height of the duct was such that combustion could be confirmed by an increase in the pressure rise along the duct length.

**(Figure 20 here)**

Results from the experiments are presented in Fig. 20(b) for an injected hydrogen mass flow of 0.40 kg/sec per metre width of the slot. Large reductions in skin friction are apparent for hydrogen injection and combustion, with the skin friction coefficient then only one quarter of the skin friction coefficient with no injection. To confirm that this effect was due to combustion, experiments were done with nitrogen test gas under the same test conditions. Although the figure shows a reduction in skin friction, due to the reduction in boundary layer densities caused by hydrogen mixing, the reductions in skin friction are much less than when combustion of the injected hydrogen took place. Figure 20(b) also displays heat transfer measurements showing that, near fuel injection, the Stanton number with fuel injection is much less that the Stanton number without fuel injection and rises towards no injection values well downstream. This reduction in heat transfer takes place in spite of the combustion heating of the boundary layer. It occurs because, by virtue of Reynold's analogy, the reduced skin friction coefficient implies a reduced Stanton number, and this effect is only partially offset by the additional combustion related heat transfer close to injection. Further downstream, more of the injected hydrogen is burned and combustion heat release has a greater relative influence on heat transfer.

The experimental results in Fig. 20(b) were compared with predictions of a numerical simulation[55, 56] and a theoretical analysis[57]. The numerical simulation employed finite rate chemistry, a $k-\varepsilon$ turbulence model, a parabolic Navier Stokes code, and assumed a uniform pressure over the surface on which the boundary layer was formed. It was generally consistent with the experimental results in predicting a reduction in skin friction in the absence of hydrogen combustion, and a large reduction in the skin friction with combustion. The low values of measured skin friction coefficient at the two downstream stations are thought to be an effect of the pressure gradients along the wall acting on the reduced wall friction. The combustion induced heat transfer reduction was also predicted satisfactorily.

The theoretical analysis[57] used a model of the turbulent boundary layer formulated by Van Driest, which represents the effect of temperature induced density changes in the boundary layer on the skin friction on a flat plate. The Van Driest model was extended by incorporating the changes in temperature and density resulting from the injection of hydrogen along the surface from an upstream slot. Combustion of the hydrogen with oxygen was assumed to take place instantaneously when the two came into contact, regardless of the temperature. This allowed the distribution across the boundary layer of the species mass fractions and the stagnation enthalpy to be determined by using the Shvab-Zeldovich scheme for coupling of these variables. The density could then be obtained as a quadratic relation in the boundary layer velocity, as in the analysis of Van Driest, but with coefficients which were different to those of Van Driest. This expression was used to yield the momentum thickness, which was differentiated with respect to the downstream distance to obtain the skin friction. As shown in Fig. 20(b), this analysis yields results which are in approximate agreement with results from the numerical simulation and the experiments.

The analysis has been employed to determine the effect on skin friction and heat transfer on a flat plate for flight velocities up to 6 km/s. It yielded values of skin friction drag which were less than half of the fuel-off skin friction drag, together with a net reduction in heat transfer when the combustion heat release in air was less than the stagnation enthalpy. The mass efficiency of hydrogen injection, as measured by effective specific impulse values, was approximately 2000 sec. Clearly, if boundary layer combustion of hydrogen can be realized over a sufficiently wide range of free stream conditions, it can be an important factor in increasing penetration of integrated scramjet configurations into the sub-orbital regime.

Investigations of the limits to the conditions under which boundary layer combustion of hydrogen will occur are in progress. Experiments using skin friction gauges[58], involving variation of the stagnation enthalpy at a Mach number of 4.3 ± 0.2, indicated that as the stagnation enthalpy fell below 5 MJ/kg the skin friction approached values obtained without combustion, and as the stagnation enthalpy exceeded 9 MJ/kg, the magnitude of the combustion induced skin friction reduction was reduced. The latter effect is thought to be due to dissociation of the combustion products. Other effects which may extend the range of conditions under which boundary layer combustion of hydrogen will occur are heating of the surface, heating of the fuel and use of ignition promoters. These effects are yet to be investigated.

Crossflow injection of hydrogen may be necessary to fuel the mainstream, and therefore an investigation was undertaken to determine the effect of cross flow injection on the hydrogen injected boundary layer[59]. The experiments were done with the apparatus of Fig. 19(a), again with five ports injecting normal to the flow 24 mm upstream of the combustion duct leading edge but also with a circumferential slot at the duct leading edge to inject hydrogen fuel in a downstream direction along the interior wall of the combustion duct. Unfortunately, numerical simulations subsequent to the experiments revealed that the thickness of the boundary layer at the combustion duct leading edge probably was not sufficient to initiate hydrogen combustion in the boundary layer. However, a reduction in skin friction due to hydrogen injection occurred and it was found that this reduction was increasingly limited as the vorticity introduced by normal injection through the upstream boundary layer was increased. Thus it appears that, in practice, realizing the substantial skin friction reductions promised by boundary layer combustion will require attention to upstream boundary layer development.

## 13. THE VALIDITY OF SHOCK TUNNEL DATA

The use of shock tunnels for studies of flows involving phenomena such as combustion at supersonic speeds, or development of inlet-combustor choking, requires no particular justification if they are seen as facilities for fundamental research only. However, if shock tunnels are to be used as an agency for transferring concepts to flight at sub-orbital speeds, it becomes important to consider their predictive capability in relation to flight, and to other facilities.

### 13.1 Effect of Freestream Oxygen Radicals

Shock tunnel operation requires the steady expansion of air from a stagnant reservoir and, if the stagnation enthalpy is high enough, some of the air molecules are dissociated. In the subsequent steady expansion through a hypersonic nozzle some of these dissociated molecules may fail to recombine, leaving atomic radicals “frozen” in the free stream flow. Frozen oxygen radicals, which occur at lower stagnation enthalpies than nitrogen radicals, were thought to offer a particular problem in flows involving combustion because they would add their heat of formation to the energy released in a combustion reaction thereby producing a combustion heat release which was artificially high. Nitric oxide (i.e. NO) molecules also exist in the free stream at relatively low enthalpies[16] and were expected to have a similar, though reduced, effect on combustion heat release.

An experimental investigation[60] was made of the effect of these frozen species on the pressure increase due to combustion of hydrogen in a constant area combustion duct. The duct had a 38 mm diameter circular cross-section, with a length of 380 mm, and tests were conducted over a range of conditions producing numerically calculated oxygen dissociation fractions up to 0.39. Flows which were essentially identical, apart from the degree of freestream oxygen dissociation, were produced by sampling the flow directly from a nozzle of area ratio 30 at a nozzle reservoir pressure of 6 MPa, and sampling the flow via an oblique shock and Prandtl and Meyer expansion from a nozzle of area ratio 108 and nozzle reservoir pressure of 40 MPa. The degree of calculated oxygen dissociation differed by a factor of the order of 10 between the two types of flow but, with combustion induced pressure increases of up to 50%, no difference was apparent in the pressure increases obtained with differing freestream dissociation levels. As combustion induced pressure increases depend on the heat release, it was concluded that the heat release was also essentially independent of freestream oxygen dissociation, at least up to the stagnation enthalpy limit of the tests, which was approximately 10 MJ/kg. Numerical simulation indicated that the lack of significant combustion heat release enhancement due to frozen species in the freestream is attributable to two effects. First, at increased levels of oxygen dissociation, the degree of dissociation in the combustion products increases, thus limiting the amount of water produced, which implies limiting the energy release. Second, some of the freestream oxygen is in the form of nitric oxide, which tends not to react due to finite rate considerations. These two effects are largely responsible for limiting the increase in combustion heat release due to the presence of frozen species in the freestream.

It might be noted that freestream oxygen radicals are expected to influence the chemical kinetics of the combustion process, and this was evident in the experiments. The higher levels of frozen species concentrations were associated with a more rapid initial pressure increase, even though the final pressure increase was unchanged.

### 13.2 Shock Tunnel vs Vitiated Blowdown Tunnel

Scramjet experiments, involving supersonic combustion, are performed in intermittent (i.e. blowdown) facilities with test times of at least a few seconds, as well as in shock tunnels. Though the two mainly operate over a different range of stagnation enthalpies, they experience some overlap in test conditions and, for validation of results from either facility, it was seen as important that those results should be consistent with one another. Therefore an experimental program was undertaken in collaboration with the National Aerospace Laboratory, Kakuda, Japan, to compare supersonic combustion pressure distributions and choking phenomena in the shock tunnel T4 with the same phenomena in a vitiated air facility at Kakuda[61]. A vitiated air facility is an intermittent facility which uses hydrogen combustion heating to raise the stagnation enthalpy of the test flow, with oxygen added to make up for that which has been burned. The experiments in both facilities were done at a precombustion Mach number of 2.4 and a stagnation temperature of 2200 K, in a rectangular duct measuring approximately 100 mm x 50 mm at injection, with a length of 400 mm to 600 mm downstream of injection. Hydrogen fuel was injected through a central strut spanning the 100 mm dimension.

Pressure distributions obtained with a constant area duct indicated that boundary layer separation and choking occurred at an equivalence ratio of approximately 0.3 for both facilities, while the pressure distributions were similar for equivalence ratios both greater than and less then the choking value. Experiments were also done with each of the 100 mm wide surfaces of the duct diverging at an angle of 1.7 degrees with respect to the duct centreline. No separation and choking occurred up to equivalence ratios of 1.05, and the duct pressure distributions were similar in the two facilities. The respective stagnation enthalpies were 2.4 MJ/kg for the shock tunnel and 2.8 MJ/kg for the vitiated air facility, which is at the lower end of the sub-orbital range. Nevertheless, it was encouraging that the two facilities yielded similar results when a relatively complicated

phenomenon, involving shock boundary layer interaction with supersonic combustion, was involved.

13.3 Shock Tunnel vs Flight. The Hyshot Experiment

The ultimate test of shock tunnel predictive capability in relation to flight is a direct comparison of shock tunnel data with data obtained in flight with the same experimental configuration and the same flow conditions. Although examples existed where flight data for external aerodynamics was compared with shock tunnel data (e.g. Ref. 10), flight data involving supersonic combustion did not exist, thus eliminating the possibility of a comparison with shock tunnel data. However, this situation changed when two sounding rocket flights became available for supersonic combustion experiments.

The sounding rockets were two-stage Terrier-Orion combinations, and were supplied by Astrotech Space Operations Inc. of the USA. As shown in Fig. 21(a), the flight began with ignition, followed by burnout and separation, of the Terrier first stage and subsequent ignition and burnout of the Orion second stage. The burnt out Orion remained attached to the experimental payload, in order to provide aerodynamic stability on re-entry to the atmosphere. The resulting flight vehicle then followed a parabolic trajectory, ascending to an altitude of 320 km before descending towards the atmosphere. While executing this manoeuvre, a control jet was activated in a "bang-bang" mode to realign the flight vehicle so that it re-entered the atmosphere with the experimental model at the nose. Re-entry was accomplished with a steep trajectory, allowing the experiment to take place over a planned period of 7 seconds as the vehicle passed from 35 km altitude to 23 km.

**(Figure 21 here)**

The experimental model is shown in Fig. 21(b). The aim of the experiment was to establish a correlation between the conditions for supersonic combustion of hydrogen fuel in the shock tunnel and in flight, and the experiment was designed to be a simple as possible, consistent with achieving this aim. A two-dimensional flow configuration was chosen, consisting of two identical flow paths, symmetrically disposed about the centreline, both of which were instrumented for pressure measurement. By arranging that fuel was injected into only one of the two combustion ducts, it was possible to compare fuel-on with fuel-off pressure distributions, and thus to make a flight to shock tunnel comparison of the effect of the hydrogen fuel mixing and combustion processes. Each inlet ramp was inclined at 18° to the centreline, and the height of the side plates at the inlet ramps was sufficient to contain the leading edge shocks for a centreline angle of attack of up to 5°. These shocks were reflected by the cowl leading edges to provide a uniform flow into the respective instrumented ducts. At the leading edge of the instrumented ducts the reflected shocks, together with the boundary layer on the inlet ramps, were dumped into gaps which existed between the inlet ramps and the leading edges of the ducts. This flow, together with the inlet flow near the sidewalls, was then dumped to the freestream via ports machined in the side walls. The boundary layer flow in the instrumented ducts thus originated at the sharp leading edges of those ducts, and thereby avoided problems likely to arise from premature boundary layer separation and choking. As shown in Fig. 21(b), the instrumented duct had 14 pressure transducers located along the duct centreline, as well as an offset pressure transducer and a heat transfer gauge.

A full scale replica of one half of the model was tested in the shock tunnel T4 before the flight, and resulting pressure distributions are compared with those obtained in flight in Fig. 22. The shock tunnel test conditions were chosen to match the ambient pressure and the flight precombustion temperatures, of 1100 K at zero angle of attack, expected for three predicted conditions occurring during descent of the flight experiment through the atmosphere. The shock tunnel Mach number was 6.4, while the expected flight Mach number was 7.6 and, to compensate for this difference, the inlet ramp angle of the shock tunnel model was reduced by one degree. During the flight

experiment, the equivalence ratio varied from 0.37 at an altitude of 35 km to 0.31 at 27 km, while it was 0.41 and 0.32 for the corresponding test conditions in the shock tunnel. As noted on Fig. 22, the flight angle of attack varied during the experiment, but the shock tunnel experiments indicated that the resulting difference between flight and tunnel values would not significantly influence the comparison of pressure distributions between the two. Unfortunately, the shock tunnel nozzle was not operated at its design condition, and this produced flow non-uniformities which are thought to be responsible for the relative unevenness of the shock tunnel pressure distributions in Fig. 22 compared with the flight pressure distributions. Allowing for this unevenness, the pressure distributions obtained in the shock tunnel are a good approximation to those obtained in flight.

**(Figure 22 here)**

The flight experiment was designed with fuel flows such that choking was avoided. However, towards the end of the experiment, the choking condition was explored by increasing the equivalence ratio. Choking occurred at an equivalence ratio of 0.33 at an altitude of 26 km, whereas the tunnel tests had predicted that, at this altitude, choking would occur at an equivalence ratio of $0.37 \pm 0.3$. Thus, as well as predicting the flight pressure distributions associated with the supersonic mixing and combustion of hydrogen, the shock tunnel could also be used to make reasonable predictions of the choking limit with that fuel. This indicates that, at least at stagnation enthalpies near 3 MJ/kg, flow fields with supersonic combustion are the same in the shock tunnel as in flight.

## 14. THE EXPANSION TUBE X3

As outlined in Section 10, the operating pressures of the shock tunnel T4 have prevented achieving the combustion heat release potential of the fuel used for an integrated scramjet configuration. This is because the boundary layer separation criteria of eqns (3) limits the inlet pressure increase and therefore limits the allowable combustion duct pressure with a given freestream static pressure. Increasing the Mach number would increase the allowable inlet compression but, as the freestream static pressure is determined by the Mach number and the shock tunnel nozzle reservoir pressure, this would be more than offset by the reduction in freestream static pressure that raising the Mach number would entail. Thus, to take advantage of the heat release potential of the fuel, the allowable combustion duct pressure should be increased by increasing the nozzle reservoir pressure.

As noted in Section 4, this has been done for shock tunnel T4. However, as there was clearly a practical limit to the maximum nozzle reservoir pressures that could be obtained with the shock tunnel, attention turned to the use of an expansion tube to generate high Mach numbers with higher freestream static pressures than shock tunnel T4. As indicated in Fig. 23(a), the use of an unsteady expansion to generate the test flow, as in an expansion tube, produces higher freestream static pressures at a given Mach number than a steady expansion. In the figure, both flows originate in the same shock tube flow, but while the unsteady flow would, in practice, be generated directly from the shock tube flow, the steady flow would be generated by reflection of the shock, and re-expansion to the Mach number $M_o$ before expansion to the Mach number $M$. Some pressure loss will occur in the process and therefore steady flow pressures will be somewhat lower than indicated by Fig. 23(a). Thus the two flows may, perhaps conservatively, be taken to originate at the same nozzle reservoir pressure, indicating that a given level of freestream static pressure may be expected at a much higher Mach number with an expansion tube than with a shock tunnel.

**(Figure 23 here)**

After study of two prototypes, the superorbital expansion tube X3, with a free piston driver, has been constructed at the University of Queensland. As shown schematically in Fig. 23(b), it consists of a free piston driver 24.6 m long followed by a shock tube 12.6 m long and an expansion

tube (or accelerating tube) 24.2 m long and 183 mm in internal diameter. The test section is in the dump tank at the end of the acceleration tube.

The facility was designed for study of phenomena associated with flight in planetary atmospheres, and time resolved records of test section pitot and static pressure in a gas mixture corresponding to the atmosphere of the moon Titan (5% methane, 95% nitrogen) are shown in Fig. 23(c). They show that an effectively steady test section flow persists for 500 microseconds at a Mach number of approximately 8.0. The ratio of the test section static pressure to the measured static pressure immediately following the primary shock was $5.8 \times 10^{-3}$, whereas the value obtained from Fig. 23(a) is $1.3 \times 10^{-2}$ for the unsteady expansion. However, Fig. 23(a) also indicates that the value of the same pressure ratio for a steady expansion to the same Mach number is $8.0 \times 10^{-4}$, implying that, in spite of the apparent flow losses in the process of producing the test flow by an unsteady expansion, it produced a static pressure more than seven times greater than would be produced by a steady expansion to the same Mach number. The pressure levels of Fig. 23(c) are somewhat less than would be desirable for research with integrated scramjet models, and modifications to the facility which are expected to allow operation at higher pressure levels are in progress. Thus the expansion tube X3 is expected to play an important role in research on integrated scramjet configurations at high Mach numbers.

## 15. SUMMARY AND CONCLUSION

The broad aim of the scramjet research at the University of Queensland has been to use a shock tunnel to explore concepts which, hopefully, will allow increasing penetration into the sub-orbital range of flight speeds with hydrogen fuel. Progress towards this aim can be followed by considering the terms on the right hand side of eqn (13), the net thrust equation. Writing this equation once more

$$C_{TN} = 2ne_n\left(\Delta Q/U^2\right)\left(1-0.5\Delta Q/U^2\right) - C_D + C_j . \qquad (13)$$

Beginning with the first term on the right hand side and noting that, to fix ideas, attention was confined to constant area combustion ducts, it was seen that, when heat release $\Delta Q$ occurred in a confined combustion wake, it was manifested as a reduction in wake Mach number and an increasing pressure along the duct, arising from the interaction of the wake with the walls of the duct. The resulting pressure distributions were consistent with a binary scaling law. The length of combustion duct required for complete combustion, and therefore maximum heat release, was not strongly influenced by the mode of fuel injection, but it increased substantially as the stagnation temperature of the fuel was increased. This work suggested that long combustion ducts were required with their attendant skin friction and heat transfer problems, and stimulated later research on means of reducing combustion duct lengths.

The factor $ne_n$ in eqn (13) represents the efficiency with which combustion heat release is converted into thrust, $n$ representing the efficiency of a one-dimensional flow combustion duct and thrust nozzle and $e_n$ the efficiency of the nozzle with respect to a one-dimensional flow nozzle. Experiments with a combustion duct-thrust nozzle combination indicated that values of the first term in eqn (13), based on the maximum theoretical and a one-dimensional thrust nozzle flow, could be realized approximately in practice. Of course, supersonic nozzle flows are not one-dimensional, but investigation of two-dimensional effects indicated that the value of $e_n$ was not too far from unity provided that nozzle expansion angles remained reasonably small, and that nozzle entry Mach numbers were not too large. An heuristic analysis of a complete scramjet configuration, based on the Busemann biplane concept, allowed a preliminary assessment of the effect of the waves that are characteristic of two-dimensional supersonic flows, and showed that a scramjet configuration should be designed for its maximum operating Mach number. This implies that designs should involve small surface angles, including small nozzle divergence angles.

The development of a force balance with sub-millisecond response times made it possible to compare eqn (13) with experiment for an integrated scramjet configuration. The force balance was based on deconvolution of the pattern of stress waves, passing into the sting support from the model, to obtain the aerodynamic forces on the model before the model reached internal stress equilibrium. Using this stress wave force balance, the net axial force acting on an integrated scramjet model was measured and compared satisfactorily with eqn (13). The design constraints on the model were such that, at the operating pressure levels of the shock tunnel, the combustion duct was not long enough, nor the pressure there high enough, to allow complete combustion of hydrogen, and it was necessary to use silane as an ignition promoter to overcome this problem. Boundary layer separation induced choking then limited operation with the resultant silane-hydrogen mixture to an equivalence ratio below 0.8, implying that the potential heat release of this fuel in eqn (13) was not realized and, as a result, thrust exceeded drag only as the stagnation enthalpy fell below 4 MJ/kg. A new design produced a model with which the cruise condition, corresponding to $C_{TN} = 0$ in eqn (13), was achieved with less than complete combustion of hydrogen fuel at a stagnation enthalpy of 3.5 MJ/kg. Essentially the same result was obtained with another model, which was used with a three component stress wave balance to measure lift and pitching moment, as well as axial force.

Experiments have been done on concepts other than the development of the combustion wake in a duct. These have been aimed at circumventing the problem of limited combustion heat release. Fuel injection on the inlet has been proven possible, and this is expected to shorten the combustion duct length by allowing mixing of the fuel with air before entering the combustion duct. Inlet injection is combined with the use of inlet compression waves and/or shock waves to create local zones of high temperature and pressure where combustion radicals are formed. Appropriately, this has been called the “radical farming” technique. A third concept, called “kinetic afterburning”, involves allowing combustion heat release to occur in the thrust nozzle, as may have happened with the hydrogen fuelled models of the previous paragraph. This technique allows higher inlet contraction ratios without choking.

Failure to maintain a net thrust in penetrating the sub-orbital regime beyond a stagnation enthalpy of 4 MJ/kg can be viewed not only as a deficiency in the first term on the right hand side of eqn (13), but also as due to the excessive value of the second term, or drag. For all three of the models mentioned above, this term was found to be nearly equally divided between inviscid and viscous drag. For ease of manufacture and analysis, simple configurations have been used for the models, and this has contributed to the inviscid drag. To enable an investigation of viscous drag a skin friction gauge was developed with a lowest natural frequency of 40 kHz, suitable for operation in the shock tunnel. Experiments on high enthalpy turbulent boundary layers in the shock tunnel confirmed that existing analytic models used to describe turbulent boundary layers would apply in the sub-orbital regime, and this was extended by experiment to include flows with combustion of hydrogen in the mainstream. In experiments with combustion in the boundary layer, the skin friction was reduced to less than one third of the value when no hydrogen was injected into the boundary layer. An analytic model was developed which took account of this effect, and predicted halving of the skin friction drag on a flat plate with injection of modest mass flows of hydrogen, at velocities up to 6 km/s, and a reduction in overall heat transfer when the combustion heat release in air was less than the stagnation enthalpy.

The validity of shock tunnel data involving supersonic combustion has been affirmed through three investigations. First, at the higher stagnation enthalpies, it was found that the theoretical presence of substantial amounts of atomic oxygen in the freestream did not have a noticeable effect on the combustion heat release. Next, a comparison between results obtained with shock tunnel and with a vitiated air facility showed that, at the relatively low stagnation enthalpies involved, flows involving supersonic combustion were the same in the two facilities. Third, at similar stagnation

enthalpies, a series of supersonic combustion flow fields obtained in flight were closely predicted by pre-flight shock tunnel experiments.

In the spirit of the title of this series, this article can be regarded as a progress report. The degree of penetration into the sub-orbital regime is governed by the net thrust equation, and initial combustion duct-thrust nozzle research suggested that this equation could be used with the full combustion heat release of hydrogen in air. However, it was found that the combustion heat release was limited with an integrated scramjet configuration, due to choking arising from turbulent boundary layer separation, and the limited operating pressures of the shock tunnel. The drag term in the net thrust equation then ensured that the net thrust did not exceed zero. This encouraged a modification to the shock tunnel which has increased operating pressures, and also led to research on other techniques of increasing the combustion heat release. However, the expected increase in combustion heat release with an integrated scramjet configuration has yet to be confirmed experimentally.

It was mentioned in the introduction that technical difficulties were inhibiting progress towards airbreathing hypersonic flight. This research has highlighted some of those difficulties. However, it has also established the value of shock tunnels in confronting those difficulties, and has led to the development of new techniques for progressing this confrontation, in the form of a stress wave force balance and a fast response skin friction gauge. It has not yet produced an integrated scramjet configuration which can achieve substantial penetration into the sub-orbital regime and, indeed, no serious attempt has been made to generate an optimum configuration for this purpose. However, when a successful attempt is made, the resulting configuration can be expected to incorporate features which will also lead to a successful flight configuration.

## ACKNOWLEDGEMENTS

The authors gratefully acknowledge the support of the Australian Research Council who, through a series of grants, has provided necessary continuity for this research. Grants from the Australian Space Office, as well as NASA grant NAGW-678, are also gratefully acknowledged. In addition, the authors acknowledge the value of discussions with colleagues, particularly those at NASA Langley Hypersonic Airbreathing Propulsion Branch. Finally, they note that this research would not have been possible without the work of many postgraduate degree candidates. They are, more or less in chronological order:- T. Cain, B. Leslie, C. Gourlay, N. Morris, M. Smart, C. Anderson, S. Sanderson, C. Stacey, R. Casey, Y. He, A. Neely, S. Tuttle, C. Brescianini, G. Kelly, R. Krek, R. Bakos, D. Buttsworth, K. Skinner, M. Wendt, P. Barker, L. Porter, L. Prucha, D. Griffin, C. Doolan, M. Pulsonetti, P. Petrie-Repar, R. Skyring, M. Kendall, A. Thomas, A. Smith, C. Goyne, I. Johnston, S. Chiu, C. Craddock, R. Palmer, O. Sudnitsin, M. Sutcliffe, M. Wegener, T. Gardner, V. Wheatley, J. Faddy, A. Bishop, D. Hunt, M. Frost, K. Austin, M. Robinson, R. Goozee, S. Rowan, B. Littleton, J. Odam, B. Stewart, M. Hayne, M. Smith, N. Truong, C. Higgins, M. Abdel-Jawad, C. Lilley, M. Suraweera, M.McGilvray.

## REFERENCES

1. Fry, R.S., “A Century of Ramjet Propulsion Technology Evolution”, Journ. Propulsion and Power, Vol. 20, No. 1, 2004, pp 27-58.
2. Anderson, G.Y., McClinton, C.R. and Weidner, J.P., “Scramjet Performance” in *Scramjet Propulsion* AIAA Progress in Astronautics and Aeronautics, Vol. 189, Ed. E.T. Curran and S.N.B. Murthy, 2000, pp 369-446.
3. Heiser, W.H. and Pratt, D.T., “Hypersonic Airbreathing Propulsion”, American Institute of Aeronautics and Astronautics, Education Series, 1994, p 535.
4. Paull, A. and Stalker, R.J. “Scramjet Testing in the T3 and T4 Hypersonic Impulse Facilities” in *Scramjet Propulsion* AIAA Progress in Astronautics and Aeronautics, Vol. 189, Ed. E.T. Curran and S.N.B. Murthy, 2000, pp 1-46.

5. Tamagno, J. and Lindemann, O., "Experimental Results on Supersonic Combustion" General Applied Science Laboratories, Ronkonkoma, New York, December, 1962.
6. Osgerby, I.T., Smithson, H.K. and Wagner, D.A., "Supersonic Combustion Tests with a Double-Oblique-Shock SCRAMjet in a Shock Tunnel", AIAA Journal, Vol. 8, No. 9, 1970, pp 1703-1705.
7. Skinner, K.A., "Mass Spectrometry of Hypersonic Combustion", Ph.D. Thesis, University of Queensland, 1994.
8. Paull, A., "A Simple Shock Tunnel Driver Gas Detector", Shock Wave Journal, Vol. 6, No. 5, 1996, pp 309-312.
9. Stacey, C.H.B, and Simmons, J.M., "Measurement of Shock-Wave/Boundary Layer Interaction in a Free-Piston Shock Tunnel", AIAA Journal, Vol. 30, No. 8, 1992, pp 2095-2099.
10. Krek, R.M. and Stalker, R.J., "Experiments on Space Shuttle Orbiter Models in a Free Piston Shock Tunnel", Aero. Journal of the Royal Aero. Soc., Vol. 96, No. 957, 1992, pp 249-259.
11. Hall, N.A., "Thermodynamics of Fluid Flow", Prentice-Hall, Inc., New York, 1951, pp 169-171.
12. Korkegi, R.H., "Comparison of Shock-Induced Two- and Three-Dimensional Incipient Turbulent Separation", AIAA Journal, Vol. 13, No. 4, 1975, pp 534-535.
13. Wendt, M.N., Jacobs, P.A. and Stalker, R.J., "Displacement Effects and Scaling of Ducted Supersonic Flames", Comb. & Flame, Vol. 115, No. 4, 1999, pp 593-604.
14. Huber, P.W., Schexnayder, C.J. Jr., McClinton, C.R. "Criteria for Self-Ignition of Supersonic Hydrogen-Air Mixtures", NASA Tech. Paper 1457, 1979.
15. Skinner, K.A. and Stalker, R.J., "Species Measurements in a Hypersonic, Hydrogen-Air, Combustion Wake", Combustion and Flame, Vol. 106, 1996, pp 478-486.
16. Skinner, K.A. and Stalker, R.J., "Mass Spectrometer Measurements of Test Gas Composition in a Shock Tunnel", AIAA Journal, Vol. 34, No. 1, 1996, pp 203-205.
17. Pulsonetti, M.V., "Scaling Laws for Scramjets", Ph.D. Thesis, University of Queensland 1997.
    *Also* Stalker, R.J. and Pulsonetti, M.V., "Experiments on Scaling of Supersonic Combustion", University of Queensland, Mechanical Engineering Research Report No. 2004/13, 2004.
18. Casey, R.T., Stalker, R.J. and Brescianini, C., "Hydrogen Combustion in a Hypersonic Airstream", Aero. Journal of the Royal Aero. Soc., Vol. 96. No. 955, pp 200-202.
19. Stalker, R.J., Morgan, R.G. and Paull, A., "A Shock Tunnel Investigation of Scramjet Performance with Partially Premixed Combustion", American Inst. Aero. And Astro. Paper No. 96-4534, 1996.
20. McIntyre, T.J., Houwing, A.F.P., Palma, R.C. Rabbath, P.A.B. and Fox, J.S., "Optical and Pressure Measurements in Shock Tunnel Testing of a Model Scramjet Combustor", Journal Prop. & Power, Vol. 13, No. 3, 1997, pp 388-394.
21. Buttsworth, D.R., "Shock Induced Mixing and Combustion in Scramjets", Ph.D. Thesis, University of Queensland, 1994.
22. Casey, R.T., "An Investigation of Supersonic and Hypersonic Hydrogen Mixing and Combustion", Ph.D. Thesis, Department of Mechanical Engineering, University of Queensland, 1991.
    *Also* Casey, R.T. and Stalker, R.J., "Hydrogen Mixing and Combustion in a High Enthalpy Hypersonic Stream", Proceedings 19$^{th}$ International Symp. On Shock Waves, Ed. Brun R. and Dumitrescu, L.Z., Marseille, France, 26-30 July 1993, Springer-Verlag, Berlin 1995, Vol. 1, pp 151-156.
23. Paull, A., "Hypersonic Ignition and Thrust Production in a Scramjet", American Inst. Aero. & Astro. Paper No. AIAA 93-2444, 1993.

24. Stalker, R.J. and Morgan, R.G., “Supersonic Hydrogen Combustion with a Short Thrust Nozzle”, Combustion and Flame, Vol. 57, 1984, pp 55-70.
25. Brescianini, C.P. and Morgan, R.G., “Numerical Modeling of Wall-Injected Scramjet Experiments”, Journal Prop. & Power, Vol. 9, No. 2, 1993, pp 169-175.
26. Wendt, M.N. and Stalker, R.J., “Transverse and Parallel Injection of Hydrogen with Supersonic Combustion in a Shock Tunnel”, Shock Waves Journal, Vol. 6, 1996, pp 53-59.
27. Morgan, R.G. and Casey, R., “Supersonic Combustion with Transverse Circular Wall Jets”, Proceedings of Tenth International Symposium on Air Breathing Engines, Nottingham, U.K. Sept. 1991. Ed. F.S. Billig. AIAA, L’Enfant Promenade, Washington DC., pp 1211-1218.
28. Wendt, M.N., Stalker, R.J. and Jacobs, P.A., “Fuel Stagnation Temperature Effects on Mixing with Supersonic Combustion Flows”, Journal Prop. & Power, Vol. 13, No. 2, 1997, pp 274-280.
29. Stalker, R.J., Truong, N.K., Morgan, R.G. and Paull, A., “Effects of Hydrogen-Air Non-equilibrium Chemistry on the Performance of a Model Scramjet Thrust Nozzle”, Aero. Journal of the Royal Aero. Soc. Vol. 108, No. 1089, 2004, pp 575-584.
30. Jacobs, P.A. and Craddock, C.S., “Simulation and Optimization of Heated, Inviscid Flows in Scramjet Ducts”, Journal Prop. & Power, Vol. 15, No. 1, 1999, pp 73-81.
31. Stalker, R.J., Morgan, R.G. and Netterfield, M.P., “Wave Processes in Scramjet Thrust Generation”, Combustion and Flame, Vol. 71, 1988, pp 63-77.
32. Smart, M.K. and Stalker, R.J., “The Glancing Interaction of a Prandtl-Meyer Expansion Fan with a Supersonic Wake”, Aero. Journal of the Royal Aero. Soc., Vol. 95, No. 942, 1991, pp 39-47.
33. Stalker, R.J., “Waves and Thermodynamics in High Mach Number Propulsive Ducts” in *High Speed Flight Propulsion Systems*, AIAA Progress in Astronautics and Aeronautics, Vol. 137, Ed. S.N.B. Murthy and E.T. Curran, 1991, pp 237-264.
34. Sanderson, S.R. and Simmons, J.M., “Drag Balance for Hypervelocity Impulse Facilities”, AIAA Journal, Vol. 29, No. 12, 1991, pp 2185-2191.
35. Tuttle, S.L., Mee, D.J. and Simmons, J.M., “Drag Measurements at Mach 5 using a Stress Wave Force Balance”, Experiments in Fluids, Vol. 19, 1995, pp 336-341.
36. Tuttle, S.L., “Measuring Thrust and Drag in a Hypersonic Impulse Facility”, Ph.D. Thesis, University of Queensland, 1996.
37. Porter, L.M., Paull, A., Mee, D.J. and Simmons, J.M., “Shock Tunnel Measurements of Hypervelocity Blunted Cone Drag”, AIAA Journal, Vol. 32, No. 12, 1994, pp 2476-2477.
38. Mee, D.J., Daniel W.J.T. and Simmons, J.M., “Three Component Force Balance for Flows of Millisecond Duration”, AIAA Journal, Vol. 34, No. 3, 1996, pp 590-595.
39. Smith, A.L. and Mee, D.J., “Drag Measurements in a Hypervelocity Expansion Tube”, Shock Waves Journal, Vol. 6, 1996, pp 161-166.
40. Paull, A., Stalker, R.J. and Mee, D.J., “Experiments on Supersonic Ramjet Propulsion in a Shock Tunnel”, Journal Fluid Mech., Vol. 296, 1995, pp 150-183.
41. Morris, N.A., “Silane as an Ignition Aid in Scramjets”, M.Eng.Sc. Thesis, University of Queensland, 1989.
42. He, Y. and Morgan, R.G., “Transition of Compressible High Enthalpy Boundary Layer Flow over a Flat Plate”, Aero. Journal of the Royal Aero. Soc., Vol. 98, No. 972, 1994, pp 25-34.
43. Stalker, R.J. and Paull, A., “Experiments on Cruise Propulsion with a Hydrogen Scramjet”, Aero. Journal of the Royal Aero. Soc., Vol. 102, No. 1011, 1998, pp 37-43.
44. Robinson, M.J., “Simultaneous Lift, Moment and Thrust Measurement on a Scramjet in Hypervelocity Flow”. Ph.D. Thesis, University of Queensland, 2003.
45. Frost, M.A., “Hyshot Scramjet Experiments in the T4 Shock Tunnel”, M.Eng.Sc. Thesis, University of Queensland, 2002.

46. Gardner, A.D., “Upstream Porthole Injection in a 2-D Scramjet Model”, M.Sc. Thesis, University of Queensland, 2001.
47. Kovachevich, A., Paull, A. and McIntyre, T., “Investigation of an Intake Injected Hot-wall Scramjet”, AIAA Paper No. 2004-1037, 2004.
48. Odam, J., “Scramjet Experiments using Radical Farming”, Ph.D. Thesis, University of Queensland, 2004.
49. Kelly, G.M., Simmons, J.M. and Paull, A., “Skin-Friction Gauge for Use in Hypervelocity Impulse Facilities”, AIAA Journal, Vol. 30, No. 3, 1992, pp 844-845.
50. Kelly, G.M., “A study of Reynolds Analogy in a Hypersonic Boundary Layer using a new Skin Friction Gauge”, Ph.D. Thesis, University of Queensland, 1994.
51. Goyne, C.P., Stalker, R.J. and Paull, A., “Transducer for Direct Measurement of Skin Friction in Hypervelocity Impulse Facilities”, AIAA Journal, Vol. 40, No. 1, 2002, pp 42-49.
52. Goyne, C.P., Stalker, R.J. and Paull, A., “Skin-Friction Measurements in High Enthalpy Hypersonic Boundary Layers”, J. Fluid Mech., Vol. 485, 2003, pp 1-32.
53. Goyne, C.P., Stalker, R.J. and Paull, A., “Shock-Tunnel Skin-Friction Measurement in a Supersonic Combustor”, Journ. Prop. & Power, Vol. 15, No. 5, 1999, pp 699-705.
54. Tanno, H., Paull, A. and Stalker, R.J., “Skin-Friction Measurements in a Supersonic Combustor with Crossflow Fuel Injection”, Journ. Prop. & Power, Vol. 17, No. 6, 2001, pp 1333-1338.
55. Goyne, C.P., Stalker, R.J. and Paull, A., “Hypervelocity Skin-Friction Reduction by Boundary-Layer Combustion of Hydrogen”, Journ. Spacecraft & Rockets, Vol. 37, No. 6, 2000, pp 740-746.
56. Brescianini, C.P., “An Investigation of the Wall-Injected Scramjet”, Ph.D. Thesis, University of Queensland, 1993.
57. Stalker, R.J., “Control of Hypersonic Turbulent Skin Friction by Boundary-Layer Combustion of Hydrogen”, Journ. Spacecraft & Rockets, Vol. 42, No. 4, 2005, pp 577-587.
58. Suraweera, M.V., Mee, D.J. and Stalker, R.J., “Skin-Friction Reduction in Hypersonic Turbulent Flow by Boundary Layer Combustion”, AIAA Paper No. 2005-0613, 2005.
59. Rowan, S.A. and Paull, A., “Performance of a Scramjet Combustor with Combined Normal and Tangential Fuel Injection”, AIAA Paper No. 2005-0615, 2005.
60. Bakos, R.J., “An Investigation of Test Flow Non equilibrium Effects on Scramjet Combustion”, Ph.D. Thesis, University of Queensland, 1994.
61. Boyce, R.R., Paull, A., Stalker, R.J., Wendt, M., Chinzei, N. and Miyajima, H., “Comparison of Supersonic Combustion Between Impulse and Vitiation-Heated Facilities”, Journ. Prop. & Power, Vol. 16, No. 4, 2000, pp 709-717.

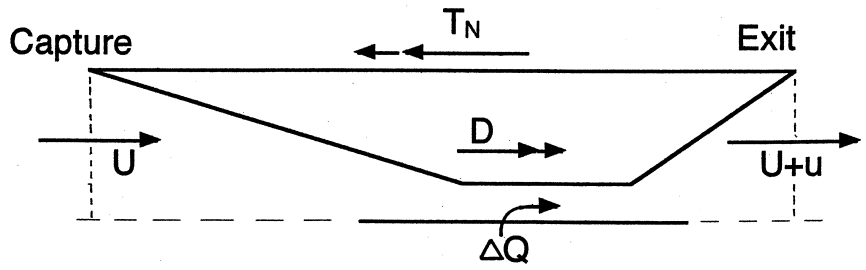


Fig.1 A notional Hypersonic Scramjet Vehicle Configuration.

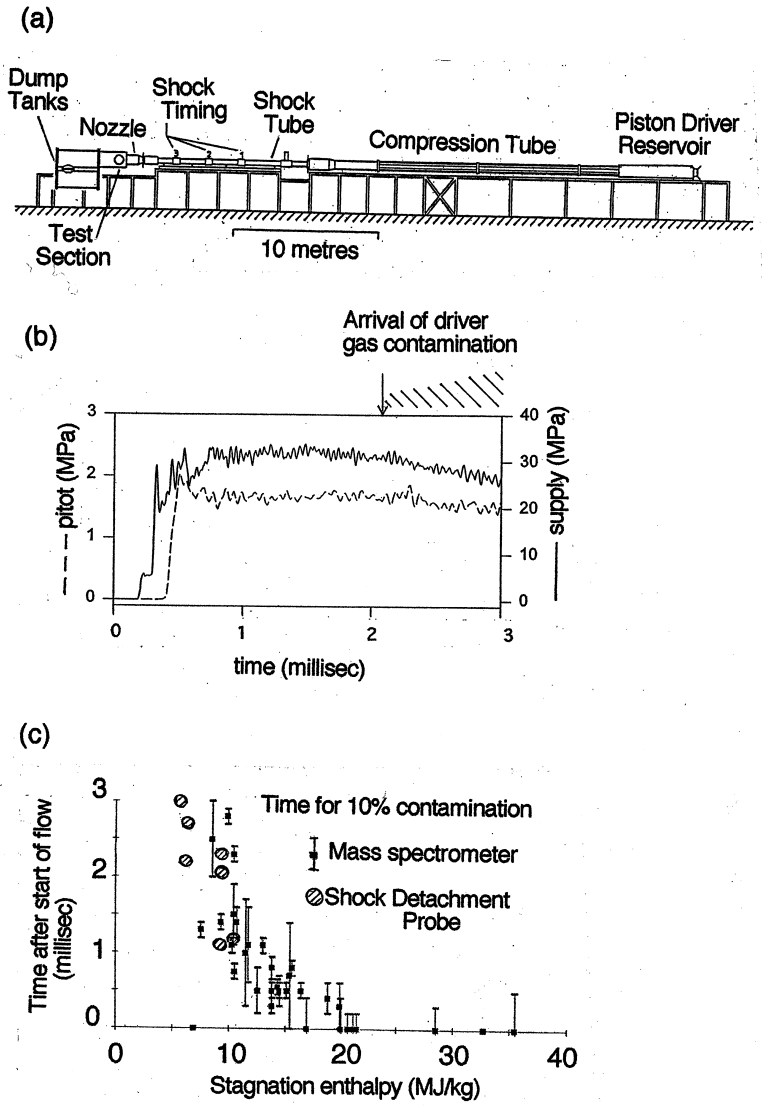


Fig.2 Free Piston Shock Tunnel T4 at the University of Queensland.
(a) General arrangement of shock tunnel.
(b) Typical records of test section pitot pressure, and of nozzle supply pressure at the end of the shock tube (stagnation enthalpy 8 MJ/kg).
(c) Test time limit due to driver gas - test gas mixing. Time for 10% molar concentration of driver gas.

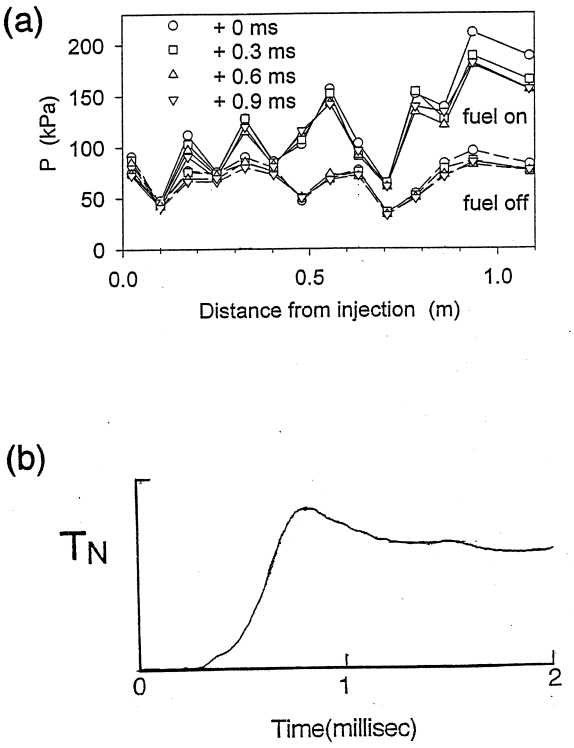


Fig.3 Typical Scramjet Measurements in Shock Tunnel T4
(a) Pressure distributions in constant area combustion duct. Hydrogen fuel. Time zero at 0.9 millisec. after shock reflection.(stagnation enthalpy = 7 MJ/kg, equivalence ratio 0.9)
(b) Time resolved thrust measured by integration over thrust surface pressure distribution.$T_N$ = nozzle thrust ( time and stagnation enthalpy as for fig.3(a))

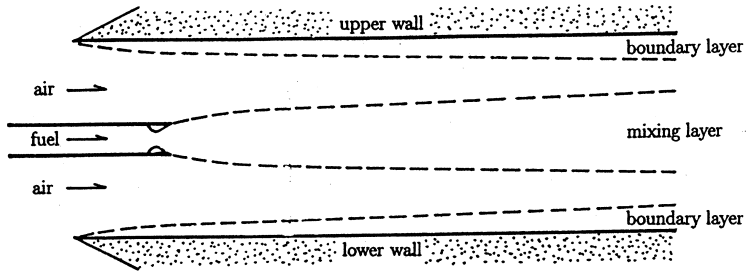


(a)

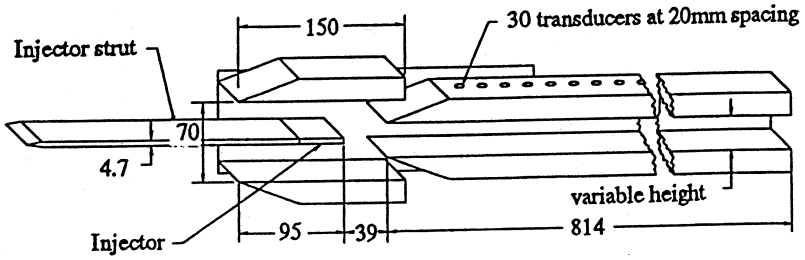


(b)

Fig.4 Combustion Wake Studies.
(a) Schematic diagram of two-dimensional combustion duct.
(b) Typical experimental two-dimensional combustion duct with near sideplate removed. Duct width 51mm. (dimensions in millimetres)

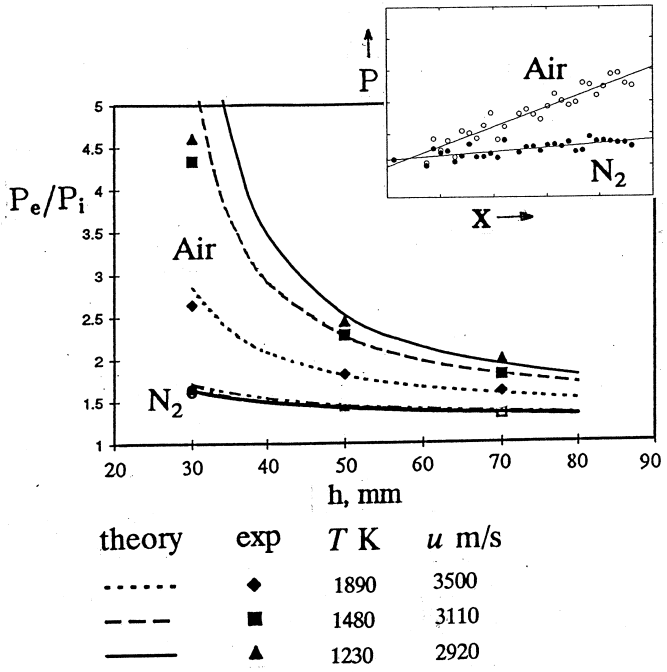


Fig.5 Displacement Effect of Combustion Wake. ( P = pressure, $P_e$ = exit pressure, $P_i$ = inlet pressure, x = distance from injector, h = duct height, T = precombustion temperature, u = precombustion velocity of air )

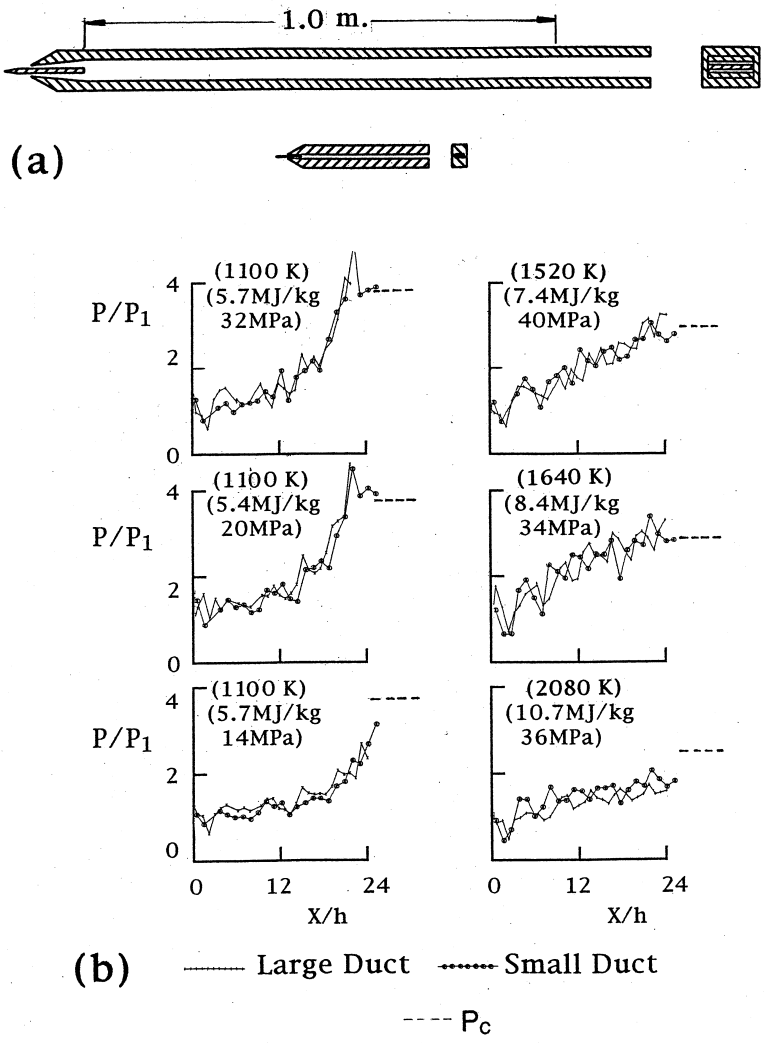


Fig.6 Scaling of Supersonic Combustion.
(a) Sketch showing relative scale of the two combustion ducts.
(b) Pressure distributions. P = pressure, $P_1$=precombustion pressure, $P_C$ =theoretical peak combustion pressure, x =distance from injector, h =duct height, precombustion temperature, stagnation enthalpy and nozzle reservoir pressure given at each condition.

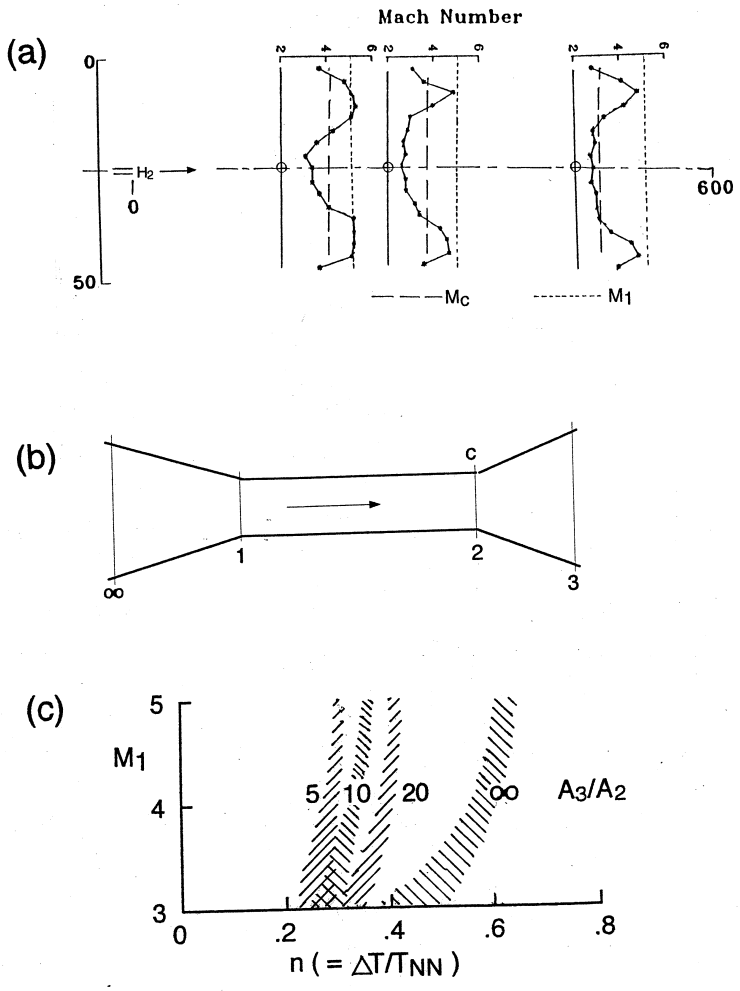


Fig.7 Thrust Producing Potential.
(a) Experimental development of combustion induced Mach number profile in constant area duct. $M_1$ =precombustion Mach number, $M_c$ =combustion induced Mach number. (dimensions in millimetres)
(b) Idealized scramjet with one-dimensional flow.
(c) Thrust producing efficiency of idealized scramjet. $M_1$ =precombustion Mach number, $\Delta T$ =thrust increment due to combustion, $T_{NN}$ = thrust if all combustion energy release is converted to stream kinetic energy.

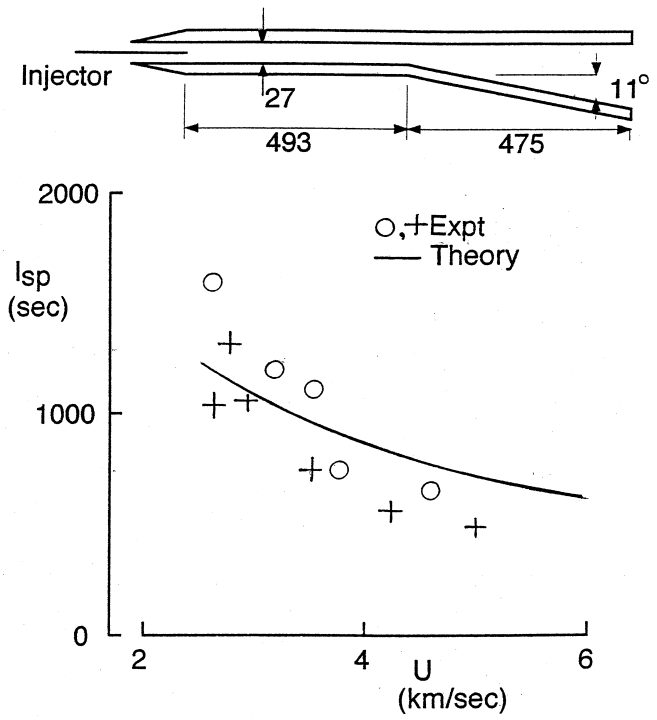


Fig.8 Incremental Specific Impulse -Stoichiometric Hydrogen.
Theory (eqn.10), n =0.32.
Experiment, circles are data for model shown, crosses are for shorter combustion duct.
(Model dimensions in millimetres)

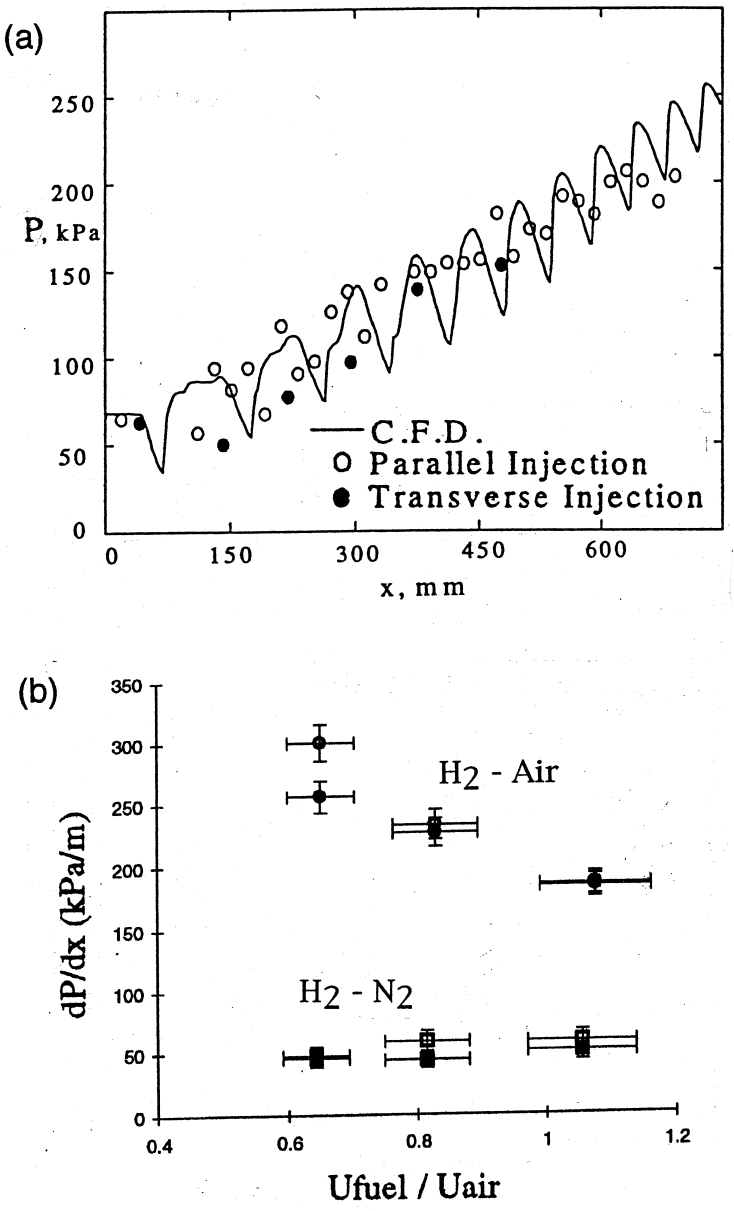


Fig.9 Fuel Injection Effects
(a) Central strut injection compared with wall orifice injection. x =distance downstream of injection.
(b) Effect of fuel stagnation enthalpy at injection, central strut injection

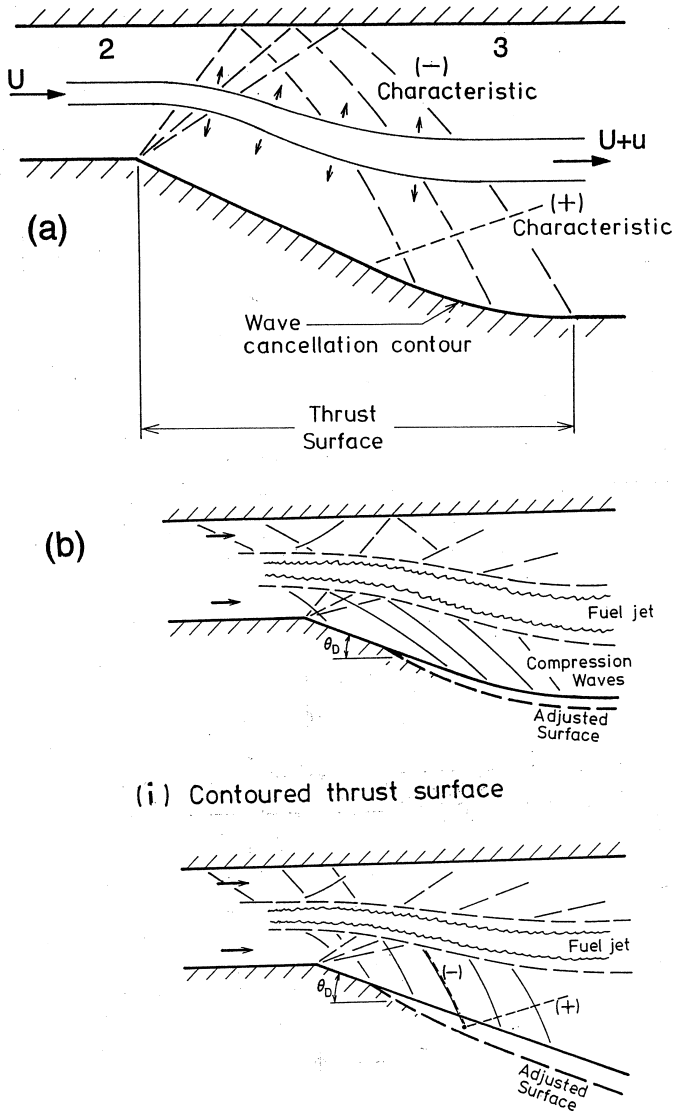


Fig.10 Thrust Nozzle with Supersonic Flow.
(a) Contoured nozzle producing uniform flow.
(b) Contoured and straight nozzles adjusted to accomodate flow with combustion.

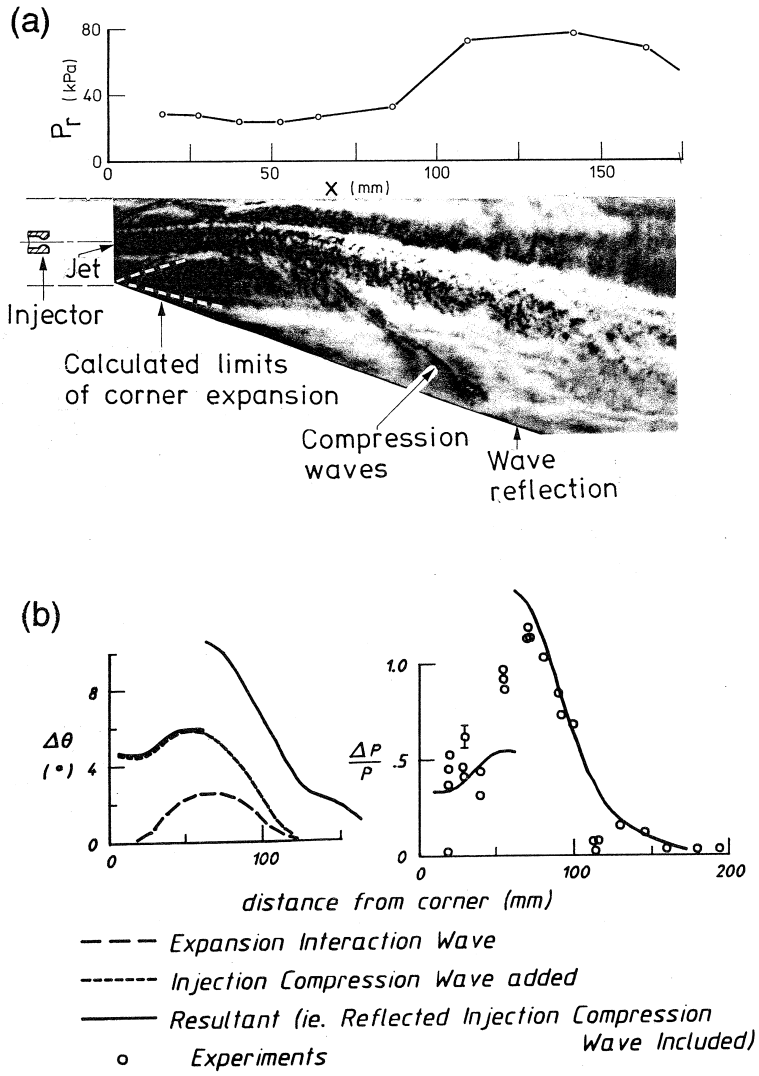


Fig.11 Thrust Generation by Combustion Wake.
(a) Schlieren photograph showing correlation between surface pressure and wave patterns. Nozzle divergence angle =19°, precombustion temperature =1300K, equivalence ratio =1.8
(b) Waves forming pressure distribution. Nozzle divergence angle =15°, precombustion temperature =1300K, precombustion velocity =2.4km/s, equivalence ratio =0.9.

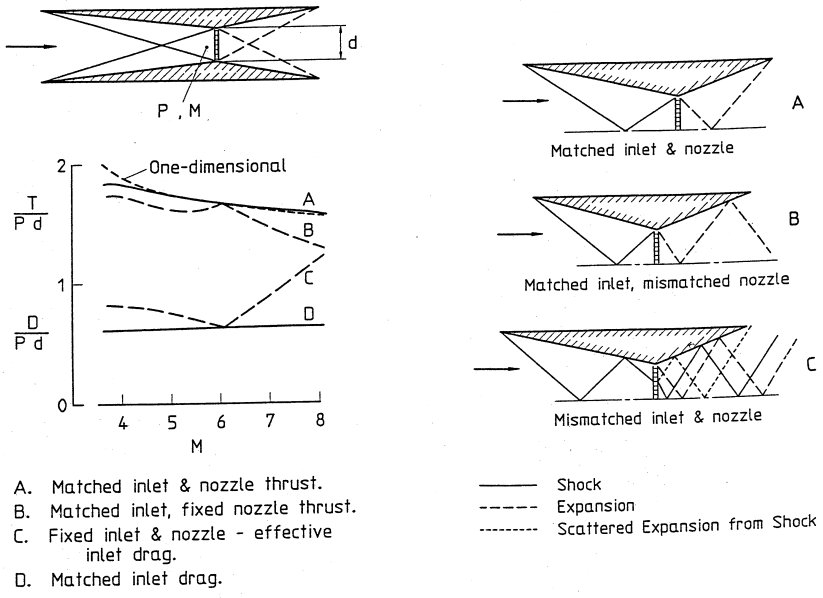


Fig.12 The Busemann Scramjet. The effect of wave patterns on the performance of a hypothetical two-dimensional scramjet. P,M =pressure and Mach number immediately before heat addition, T =nozzle thrust, D =inlet drag.

(a)

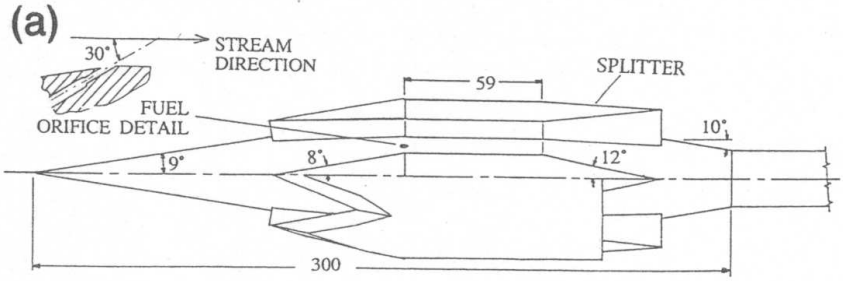


(b)

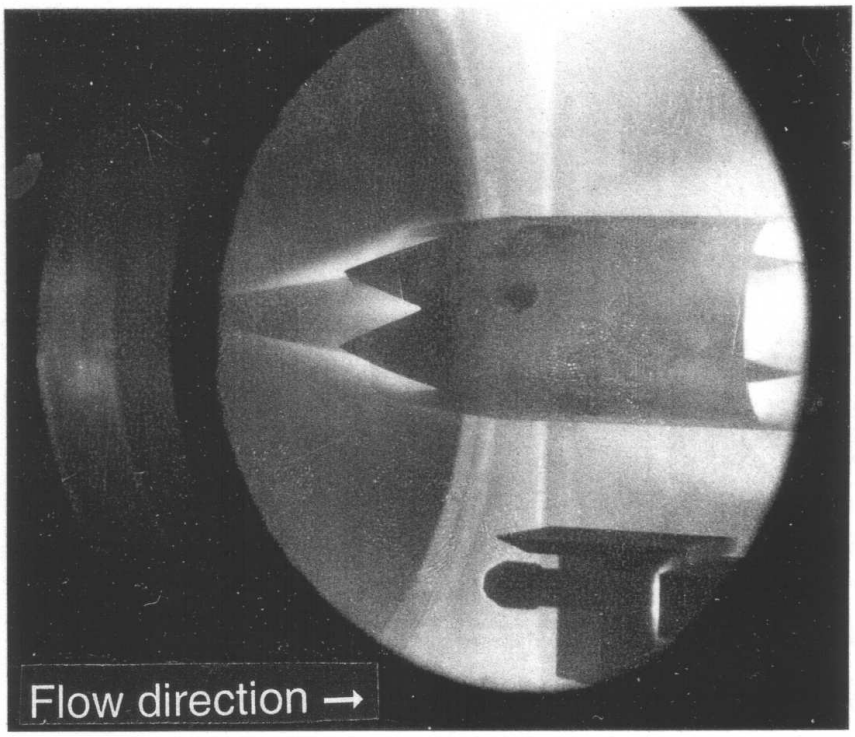


Fig.13 Integrated Scramjet Model.
(a) Model detail (dimensions in millimetres)
(b) Time integrated photograph of model during a test at stagnation enthalpy 3MJ/kg. (forecone luminosity due to trace impurities in test flow, luminosity from combustion at downstream end of cowl.)

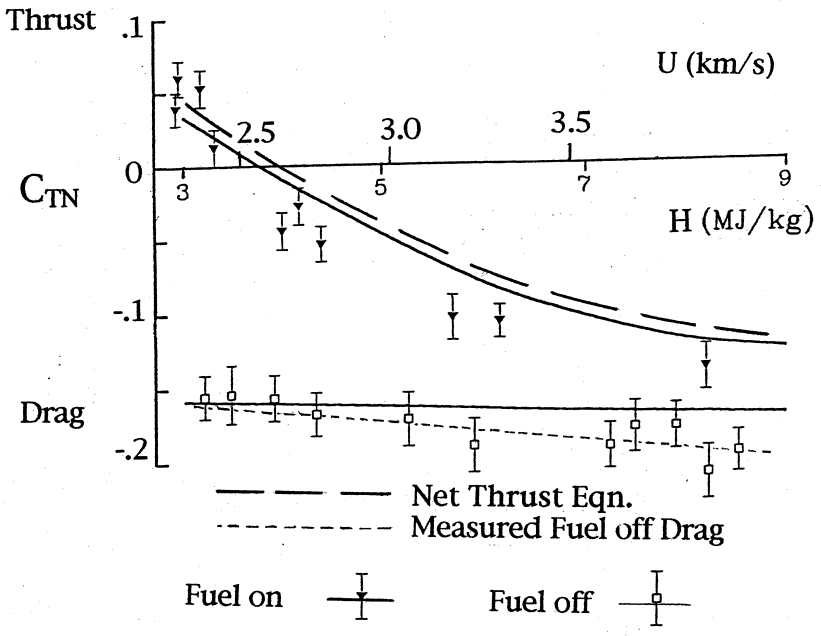


Fig.14 Performance of Axisymmetric Integrated Scramjet Model in Shock Tunnel.

Net Thrust Equation:

$$C_{TN} = 2ne_n(\Delta Q/U^2)(1 - 0.5\Delta Q/U^2) - C_D + C_J$$

$C_D$ = measured fuel off drag coeff,

$C_J$ = fuel injection thrust coeff,

H = stagnation enthalpy

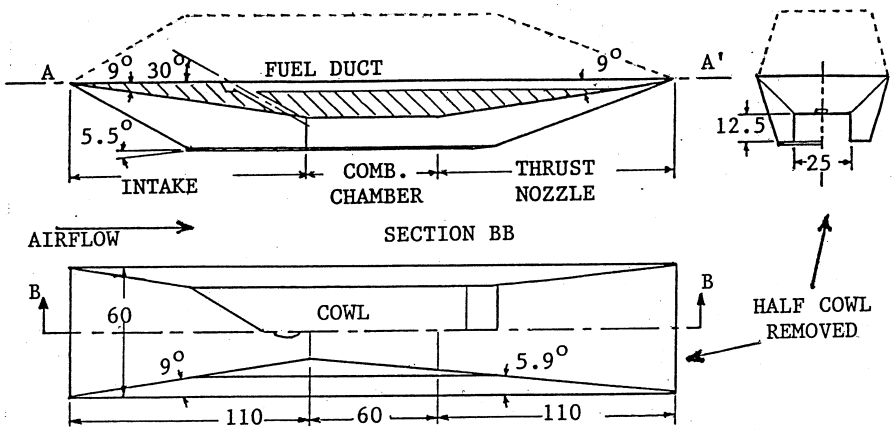


Fig.15 Hydrogen Fuelled Scramjet Cruise Model.
Model symmetrical about plane AA'.
(dimensions in millimetres)

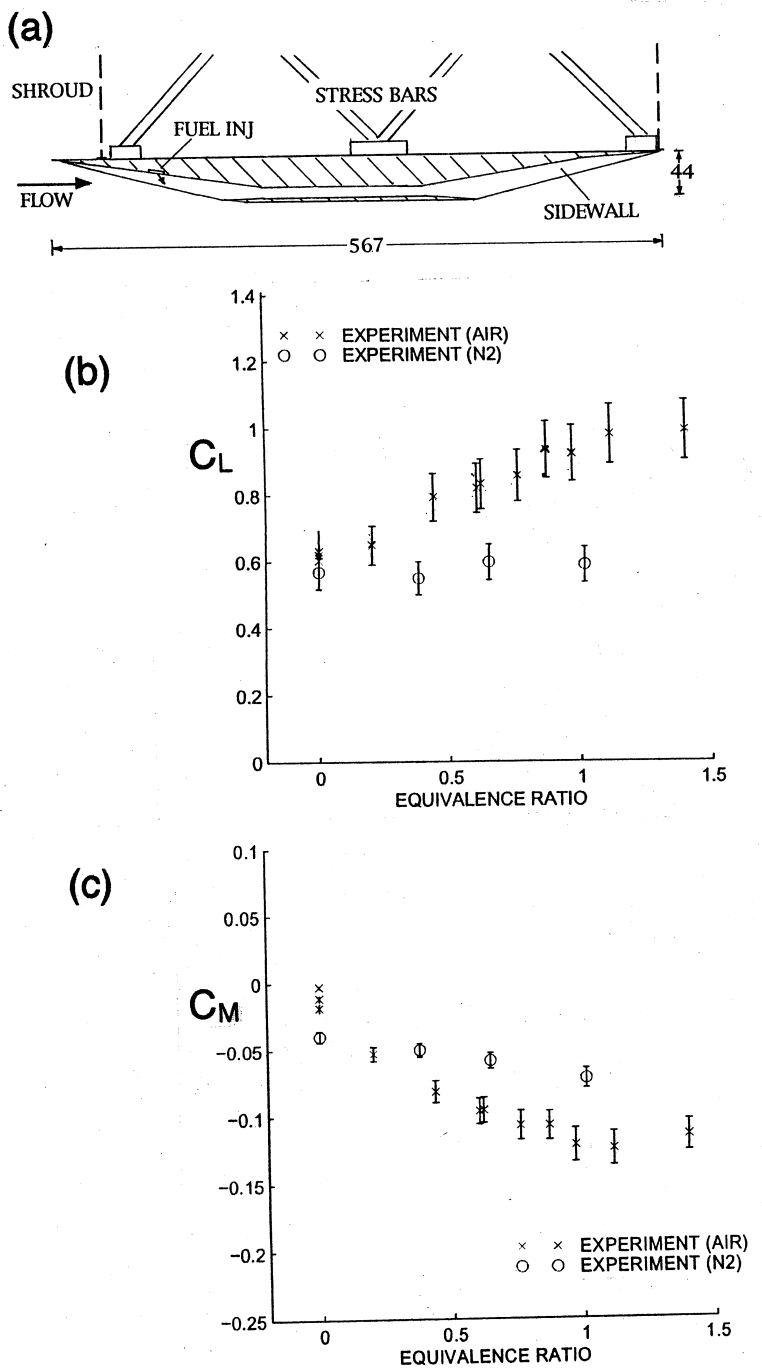


Fig.16 Three Component Force Balance with Scramjet Model.
(a) Model detail (dimensions in millimetres)
(b) Lift increase due to combustion.
$C_L$ = lift coefficient
(c) Pitching moment change due to combustion.
$C_M$ = pitching moment coefficient, based on model length

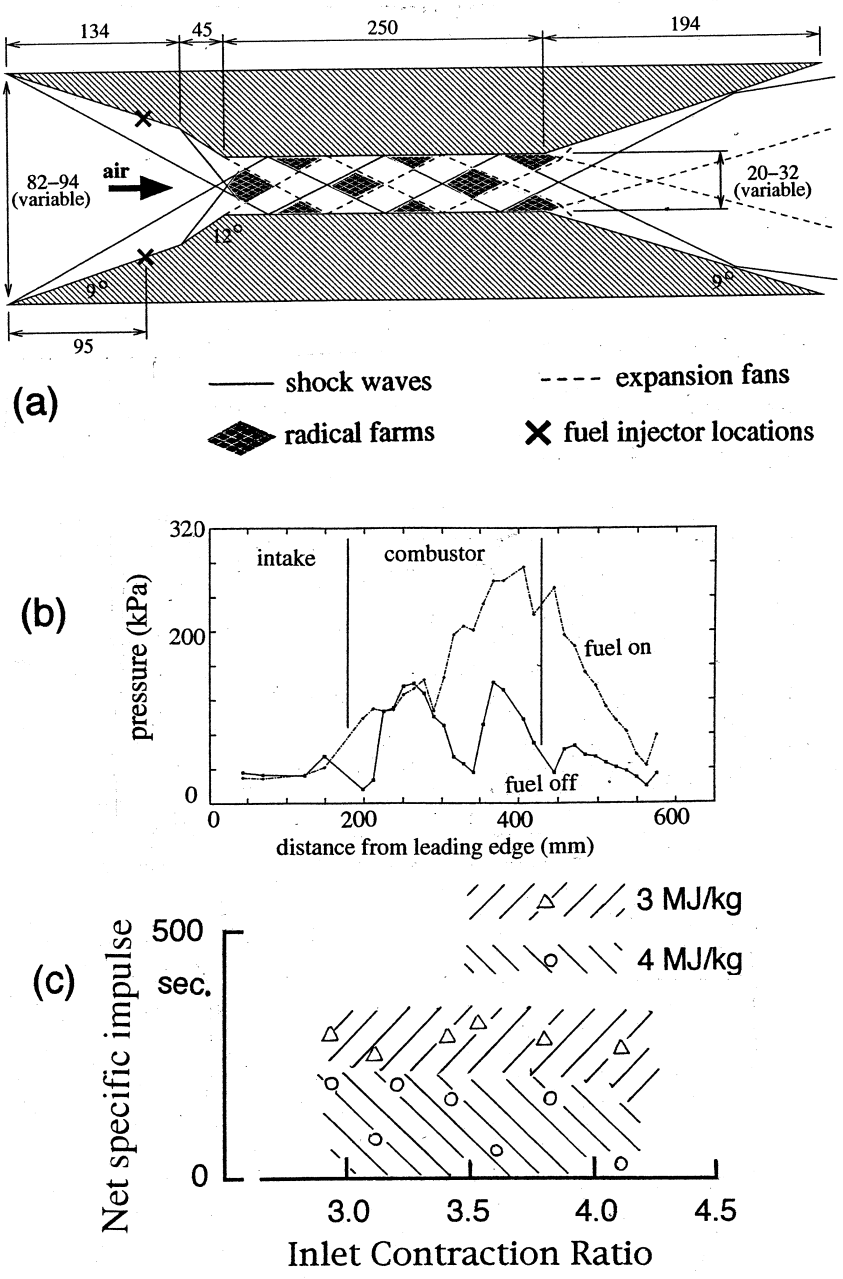


Fig.17 Experiments on Radical Farming
(a) Model dimensions (millimetres)
(b) Surface pressure distributions. Stagnation enthalpy =4MJ/kg, equivalence ratio =0.8, inlet contraction ratio =2.9.
(c) Internal flowpath performance.

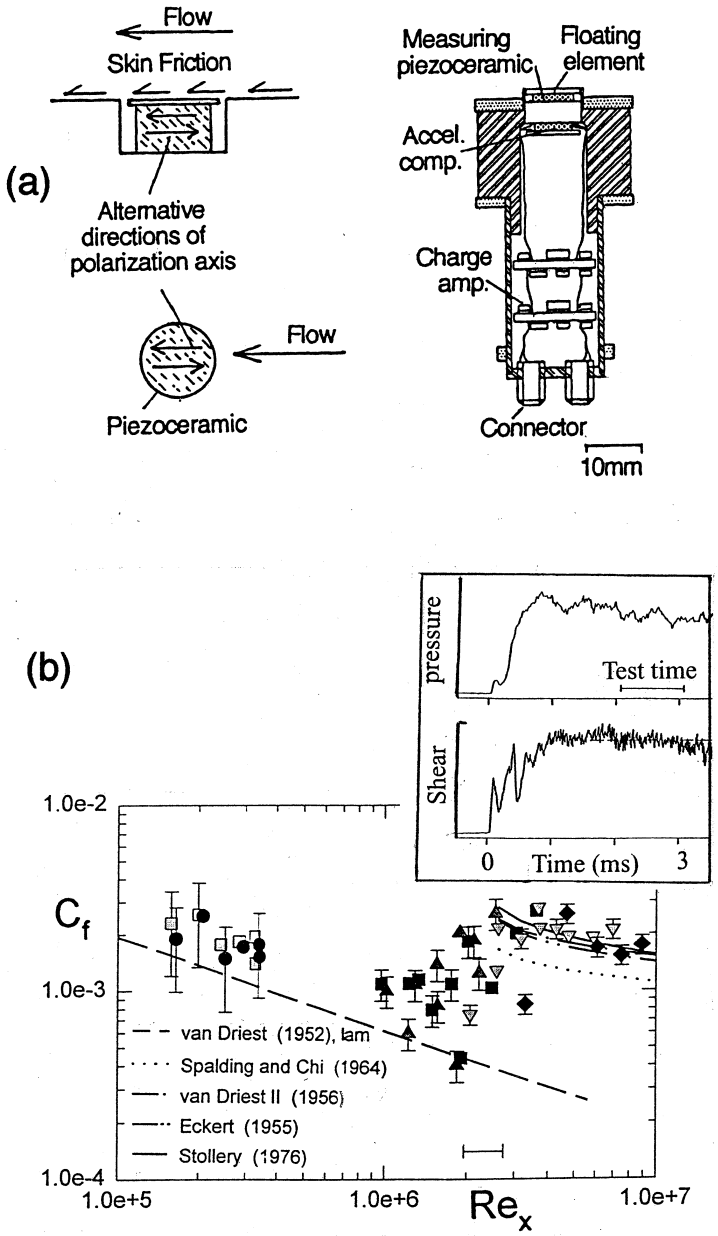


Fig.18 Skin Friction Gauge.
(a) Principle of operation and design layout.
(b) Typical skin friction measurements, stagnation enthalpy =6.5MJ/kg. Inset - typical gauge response, stagnation enthalpy 3.4MJ/kg.

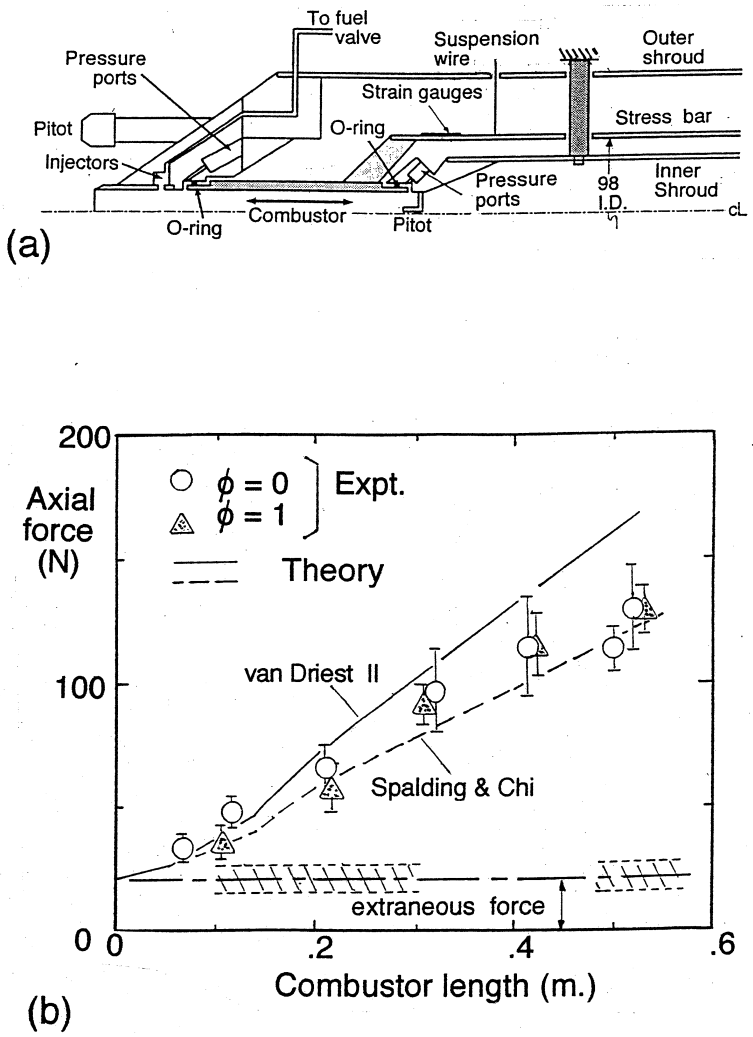


Fig.19 Skin Friction Drag on Combustion Duct.
(a) Model assembly (dimensions in millimetres)
(b) Effect of combustion duct length on skin friction drag.

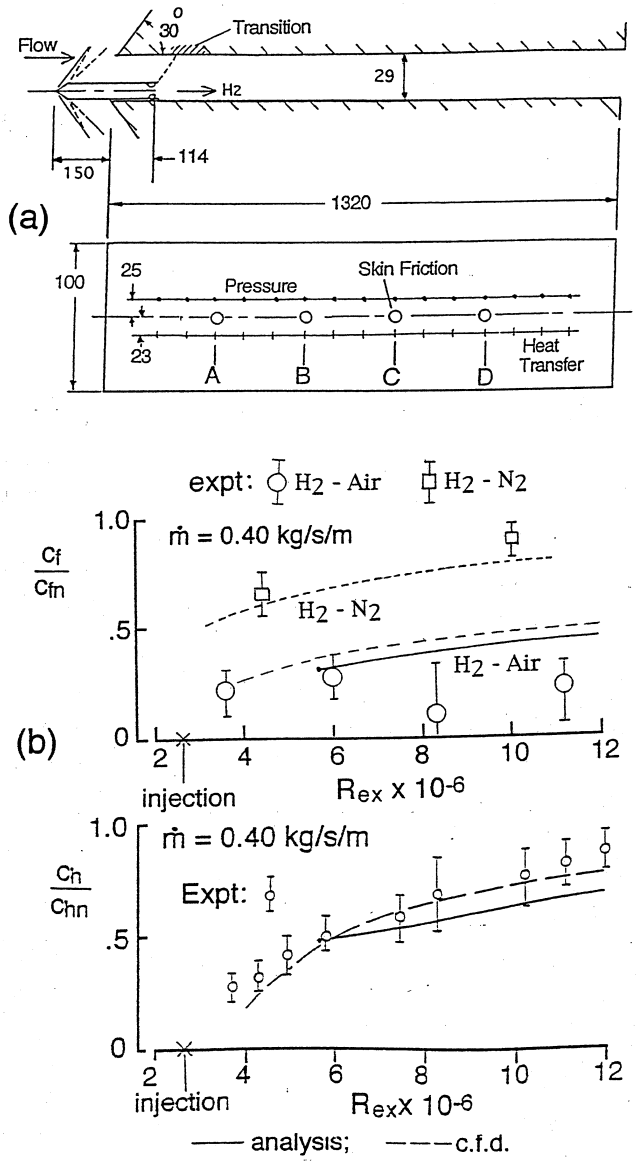


Fig.20 Turbulent Skin Friction Reduction by Boundary Layer Combustion.

(a) Experimental duct details (dimensions in millimetres. Note: scale of horizontal and vertical dimensions differ)

(b) Skin friction and heat transfer measurements,

$c_f$, $c_{fn}$ =skin friction coefficient with and without $H_2$ injection respectively.

$c_h$, $c_{hn}$ =Stanton number with and without $H_2$ injection respectively.

$\dot{m}$ = $H_2$ mass flow.

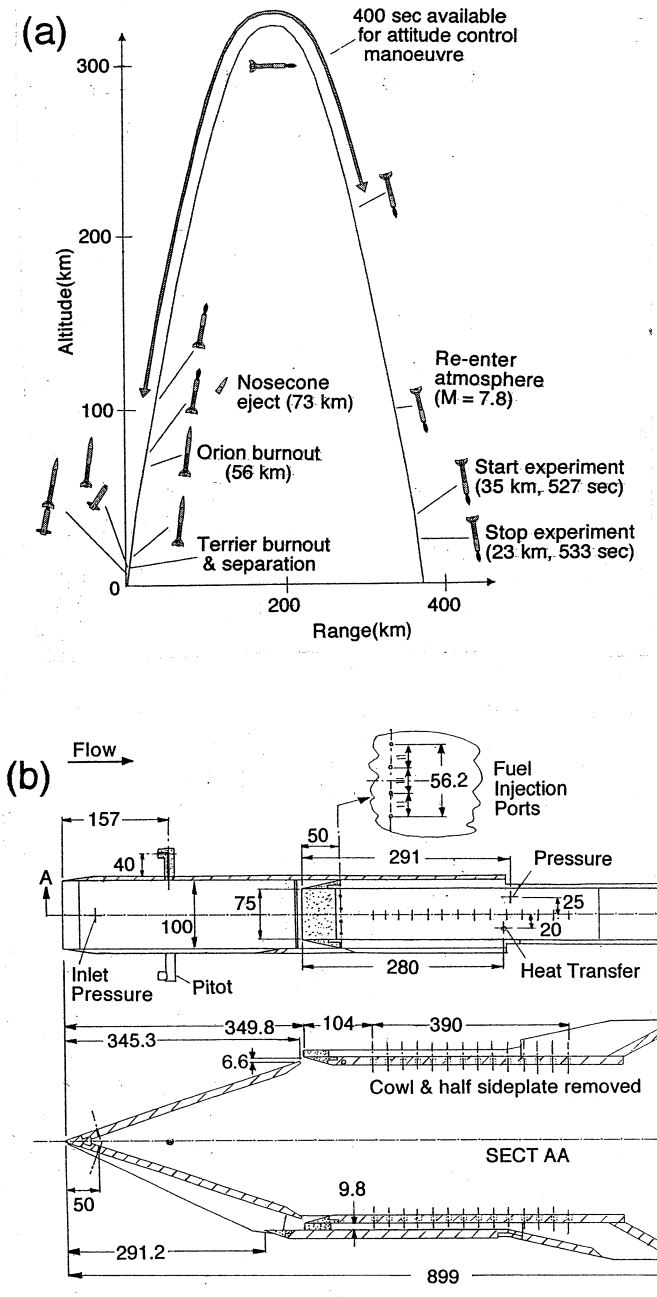


Fig.21 HyShot Flight Experiment.
(a) Flight trajectory
(b) Model detail (dimensions in mm )

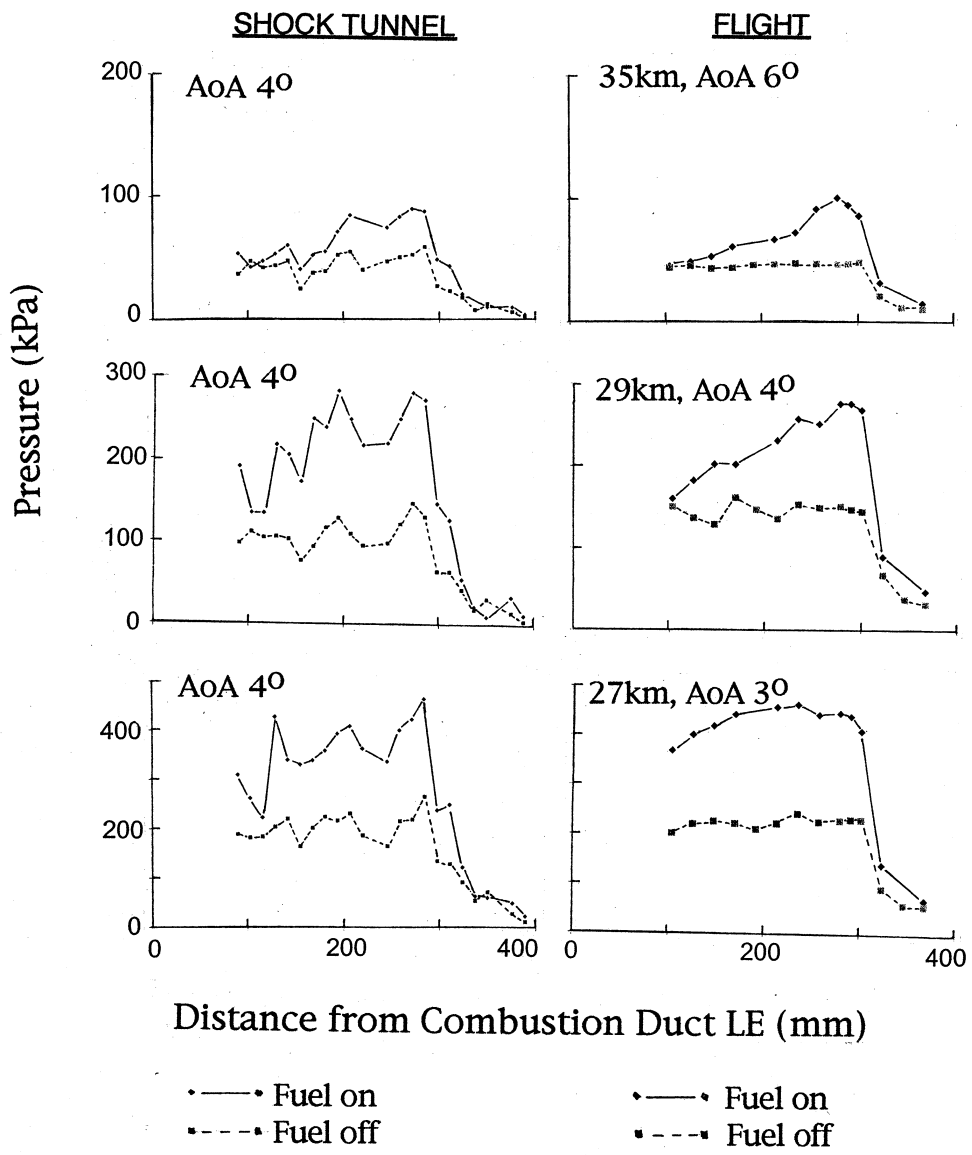


Fig.22 Comparison of Shock Tunnel and Flight Combustion of Hydrogen. Flight altitude in kilometres, AoA = angle of attack.

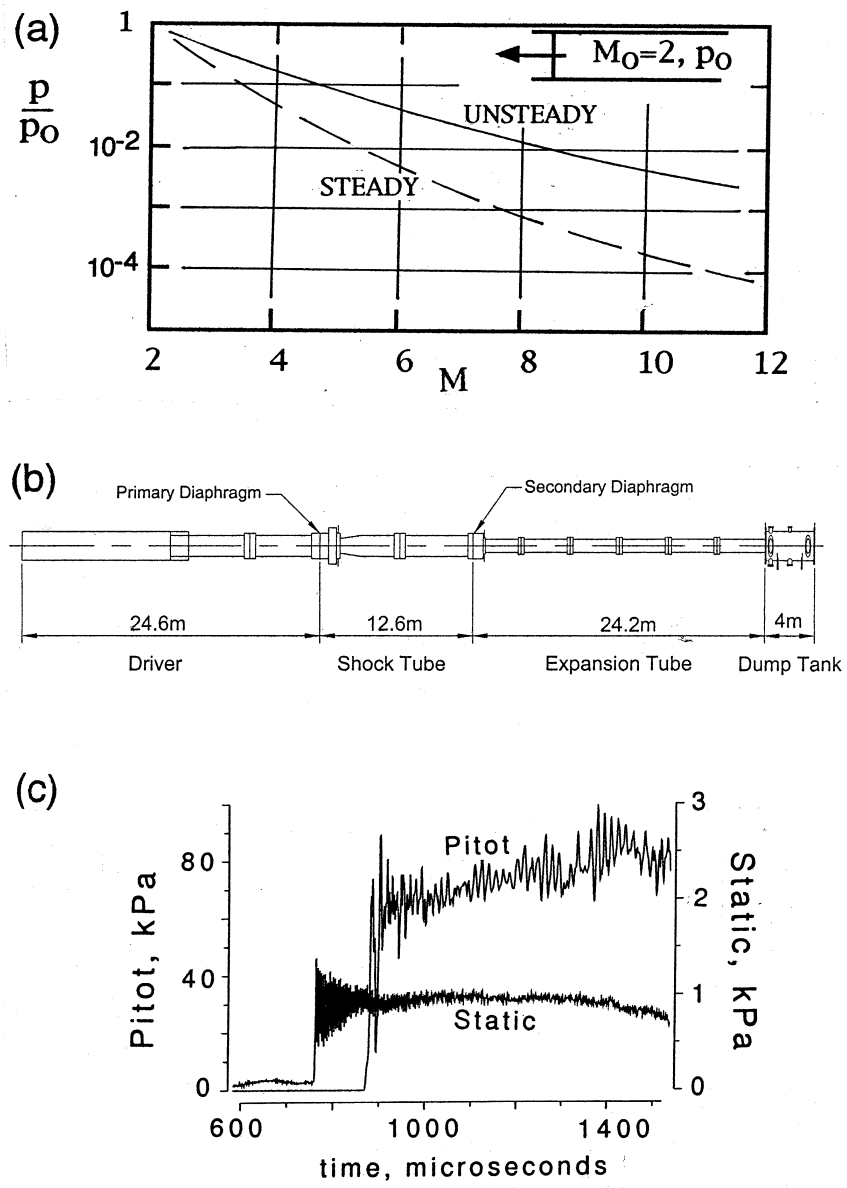


Fig.23 Extending the Scramjet Testing Envelope -the Expansion Tube.

(a) Benefit of unsteady expansion. M,p =Mach number and pressure after expansion from $M_o$ and $p_o$, $\gamma = 1.4$.

(b) Expansion tube X3.

(c) Test section pressure records in X3. Velocity =5.4km/s.